A brain-accessible peptide modulates stroke inflammatory response and neurotoxicity by targeting BDNF-receptor TrkB-T1 specific interactome

Lola Ugalde-Triviño[1], Gonzalo S. Tejeda[2,†], Gema M. Esteban-Ortega[1,†,*] and Margarita Díaz-Guerra[1]

[†]These authors contributed equally to this work

*Present address: Centro de Biología Molecular Severo Ochoa (CBMSO), Consejo Superior de Investigaciones Científicas-Universidad Autónoma de Madrid, Nicolás Cabrera,1. Madrid 28049, Spain

1 Instituto de Investigaciones Biomédicas Sols-Morreale (IIBM), Consejo Superior de Investigaciones Científicas-Universidad Autónoma de Madrid, Madrid 28029, Spain

2 Institute of Molecular, Cell and Systems Biology, College of Veterinary Medical and Life Science, University of Glasgow, Glasgow, UK

Correspondence to: Margarita Díaz-Guerra

Instituto de Investigaciones Biomédicas Sols-Morreale, Consejo Superior de Investigaciones Científicas-Universidad Autónoma de Madrid (CSIC-UAM). Arturo Duperier, 4, Madrid 28029, Spain

E-mail: mdiazguerra@iib.uam.es

Abstract

Glia reactivity, neuroinflammation and excitotoxic neuronal death are central processes to ischemic stroke and neurodegenerative diseases, altogether a leading cause of death, disability, and dementia. Given the high incidence of these pathologies and the limited efficacy of current treatments, developing brain-protective therapies that target both neurons and glial cells is a priority. Truncated neurotrophin receptor TrkB-T1, a protein produced by these cell types, plays relevant roles in excitotoxicity and ischemia. We hypothesized that interactions mediated by isoform-specific TrkB-T1 sequences might contribute to neurotoxicity and/or reactive gliosis, thus representing potential therapeutic targets.

Methods

We designed cell-penetrating peptides containing TrkB-T1 isoform-specific sequences to: 1) characterize peptide delivery into rat primary cortical cultures and mice brain cortex; 2) isolate and identify the isoform interactome in basal and *in vitro* excitotoxic conditions; 3) analyze peptide effects on neuroinflammation and neurotoxicity using primary cultures subjected to excitotoxicity or *in vivo* in a mouse model of ischemia.

Results

We identify here the TrkB-T1-specific interactome, poorly described to date, and demonstrate that interference of these protein-protein interactions using brain-accessible TrkB-T1-derived peptides can reduce reactive gliosis and decrease excitotoxicity-induced damage in cellular and animal models of stroke, where treatment reduces the infarct volume in male and female mice.

Conclusions

The crucial role of TrkB-T1 in modulating microglia and astrocyte reactivity indicates that isoform-derived peptides hold promise for the development of therapies for human stroke and other excitotoxicity-associated pathologies.

Running title: TrkB-T1 as a target for stroke therapy

Keywords: cell-penetrating peptides, excitotoxicity, inflammatory response, interactome, neurodegeneration, neuroprotection

Introduction

Stroke is a leading cause of death, disability, and dementia. Ischemic stroke, which accounts for approximately 85% of total cases, results from the blockage of a cerebral blood vessel, leading to reduced nutrient and oxygen levels in the affected area, culminating in neuronal death and irreversible brain damage. After an insult, two damaged areas can be distinguished, the infarct core and the penumbra. The infarct contains irreversible damaged tissue while the penumbra is functionally impaired but metabolically active. Consequently, the penumbra has become a neuroprotection target, although, if no therapy is applied, neurons can suffer secondary death mainly due to excitotoxicity. This process results from overactivation of glutamate receptors, particularly N-methyl-D-aspartate receptors (NMDARs), followed by massive influx of Ca^{2+} ions and subsequent disruption of ion homeostasis. Another contribution to ischemic stroke pathophysiology is the inflammatory response [1]. Resident immune cells, including astrocytes and microglia, result activated in the acute phase, preceding passage of circulating immune cells to injured tissue across the damaged blood–brain barrier (BBB). Reactive astrogliosis, a process occurring in the peri-infarct environment, implies a dramatic cellular transformation that increases proliferation/migration, modifies morphology and leads to upregulation of genes such as *Gfap,* encoding glial fibrillary acidic protein [2]. A subtype of reactive astrocytes loses homeostatic properties and experiences a pro-inflammatory gain of function with detrimental effects on neuronal and oligodendrocyte survival [3-5]. Neuronal function is also regulated by microglia through neurotrophic factors release or specialized junctions formed by microglia processes with synaptic elements or neuronal bodies [6]. Interestingly, a cross-talk between astrocyte and microglia activation is established in the CNS and, for example, neurotoxic reactive astrocytes are induced by microglia secretion of cytokines such as complement component 1q (C1q) [7].

Mechanisms underlying excitotoxicity and reactive gliosis are still largely undefined although they might unveil novel targets for stroke therapy. Conventional pharmacological thrombolysis and mechanical thrombectomy have significant limitations and benefit only a small proportion of patients [8]. Therefore, we need to identify new candidates and develop strategies ideally targeting the different pathological processes and cell types involved in stroke. Signaling by brain-derived neurotrophic factor (BDNF)-binding to its high-affinity transmembrane receptor, tropomyosin-related kinase B (TrkB), becomes profoundly aberrant in stroke [9,10]. In physiological conditions, BDNF is produced by multiple cells, including neurons and glia [11], and promotes neuronal maturation, differentiation, survival and synaptic function, among other processes. Different TrkB isoforms are produced by gene *Ntrk2* alternative splicing [12], full-

length TrkB (TrkB-FL) and truncated TrkB-T1 being the major murine cortex isoforms [13]. TrkB-T1 is the predominant isoform in the adult nervous system where it is mostly expressed by astrocytes and, secondarily, neurons. In contrast, TrkB-FL is almost exclusively expressed in neurons [14]. BDNF-binding to TrkB-FL induces receptor dimerization, increased tyrosine kinase (TK) activity and transphosphorylation, leading to activation of interconnected signaling pathways that, altogether, stimulate processes central to CNS functioning. These pathways include the activation of prosurvival transcription factors (TFs) such as cAMP response element-binding protein (CREB) [15] and myocyte enhancer factor 2 (MEF2) [16,17], which regulate a wide array of genes, including those encoding BDNF [18-20], TrkB [21] and certain NMDAR subunits [22]. In neurons, BDNF can also bind to TrkB-T1, truncated isoform lacking the TK region and traditionally considered as a dominant-negative receptor inhibiting BDNF-signaling [23]. TrkB-T1 expressed in hippocampal astrocytes also participates in fine-tuning of neurotrophin-signaling by BDNF storage and translocation after BDNF/TrkB-T1 internalization [24].

In response to BDNF, TrkB-T1 also regulates important astrocyte functions including calcium release from intracellular stores [25], glycine [26] and gamma aminobutyric acid (GABA) transport [27], and cell maturation [28] and morphology [29]. These TrkB-FL-independent actions might rely on interactions established by a highly conserved and isoform-specific TrkB-T1 C-ter sequence (FVLFHKIPLDG) [13,23] although the only TrkB-T1-interacting protein previously identified is RhoGDP dissociation inhibitor 1 (RhoGDI1), found in astrocytes [29]. This protein controls the family of Rho GTPases, regulatory proteins that link surface receptors to cytoskeleton organization, regulation of gene transcription and neuronal survival/death [30]. TrkB-T1 expression is upregulated in multiple disorders, including stroke, spinal cord injury, several neurodegenerative diseases (NDDs) or Down syndrome [31]. In stroke, while TrkB-FL decreases in the infarct core, TrkB-T1 levels increase in the surrounding astrocytes [32], promoting ischemic damage and contributing to oedema formation [33]. This TrkB imbalance could be reproduced in a model of *in vitro* excitotoxicity, where it significantly contributed to neuronal death [9]. This is important because excitotoxicity is not only a mechanism central to stroke but it is also associated to other acute (hypoglycemia, acute trauma) or chronic CNS disorders such as NDDs [34]. Three excitotoxicity-induced mechanisms contribute to aberrant TrkB function: (1) modification of normal ratio of isoform mRNAs, favoring TrkB-T1 mRNA [9,35]; (2) TrkB-FL calpain cleavage, resulting in a non-functional truncated receptor similar to TrkB-T1 and a cytosolic TK-containing fragment [36]; (3) regulated intermembrane proteolysis (RIP) of both isoforms by sequential action of metalloproteinases (MPs), shedding

identical ectodomains acting as BDNF scavengers, and γ-secretases, releasing the isoforms intracellular domains (ICDs) [36]. RIP is a major mechanism of TrkB-T1 regulation both *in vitro* and after ischemia while it is only secondary for TrkB-FL [36]. Similarly to other RIP substrates, TrkB-T1-ICD could trigger local signaling or modify gene expression after nuclear translocation [37]. Altogether, these pathological mechanisms lead to abnormal BDNF/TrkB-signaling which contributes to excitotoxicity, pointing to TrkB-FL and TrkB-T1 as relevant therapeutic targets for treatment of stroke and excitotoxicity-associated pathologies. We have previously designed a cell-penetrating peptide (CPP) able to cross the BBB and plasma membrane that interferes excitotoxicity-induced TrkB-FL retrograde transport to the Golgi complex, secondarily preventing receptor processing [38] and organelle disruption [39], a neurodegeneration hallmark. In a model of ischemia, this neuroprotective peptide efficiently reduces infarct size and neurological damage [38]. The significant role of TrkB-T1 in excitotoxicity, coupled with the potential to target both neurons and glial cells, strongly justifies the development of alternative or complementary therapeutic strategies focused on this isoform. In order to that, we relied again on CPPs since they have important advantages for non-invasive delivery of therapeutic compounds to the CNS: translocation capacity across cell membranes, ability to infiltrate many different cell types, large cargo capacity and low toxicity [40,41]. Although the pharmacokinetic properties of CPPs present some limitations, promising results have been recently obtained in a phase 3 clinical trials for acute ischemic stroke [42,43].

Here, we hypothesize that isoform-specific TrkB-T1 interactions might play a relevant role in neurotoxicity and/or reactive gliosis. Therefore, their interference might prevent those pathological processes and decrease the ischemic damage. We have designed TrkB-T1-derived CPPs to isolate and identify the isoform interactome in basal and excitotoxic conditions. We also demonstrate that these peptides regulate neuroinflammation and are neuroprotective against *in vitro* or *in vivo* excitotoxicity, suggesting that they might be relevant for therapy of human stroke and other pathologies associated to excitotoxicity and neuroinflammation.

Methods

Reagents and resources are described in the Table S1.

Experimental models

Animal procedures were performed following European Union Directive 2010/63/ EU and approved by ethics committees from CSIC and Comunidad de Madrid (Ref PROEX 276.6/20).

Mice model of ischemia by photothrombosis

Permanent focal ischemia was induced in cerebral cortex of adult male and female mice by microvascular photothrombosis as described [38] with modifications. Brain injury involves vascular endothelium damage and platelet activation, followed by microvascular thrombotic occlusion of a particular region [44] selected for illumination using a stereotaxic frame. Coordinates were +0.2 AP, +2 ML relative to Bregma and damaged area corresponded to primary motor and somatosensory cortex. For neuroprotection, a single dose (3 nmol/g) of peptides TMyc or $TT1_{Ct}$ (see below) was administered 1 h after damage initiation. Further details of the procedures, including measurement of infarct volume and evaluation of motor coordination and balance, are detailed as Supplementary material.

Primary cultures of rat cortical neurons and treatment

Cultures were prepared from cerebral cortex of 18-day-old Wistar rat embryos, both genders indistinctly included [45]. Unless otherwise indicated, glial growth was inhibited after 7 days *in vitro* (DIVs), experimental treatments taking place after 12 DIVs. These cultures present a high percentage of neurons, combined with glial cells, mostly astrocytes [9]. To induce excitotoxicity, cultures were incubated with NMDA (100 μM) and its co-agonist glycine (10 μM), herein denoted simply as NMDA, which induce a strong excitotoxic response in mature neurons but have no effect on astrocyte viability [46,47]. When indicated, cultures were preincubated for 30 min with indicated concentrations of Tat-derived CPPs before NMDA treatment, peptides being kept in the medium along treatment. Total cell or neuronal viability assessment was established by the thiazolyl blue formazan (MTT) reduction assay. Further details are provided as Supplementary material.

Pull down assays and proteomic analysis

Cultures incubated with biotinylated peptides and treated as indicated were lysed at 4°C in NP-40 lysis buffer. Equal protein amounts were combined with streptavidin-agarose beads and incubated for 1.5 h for specifically-bounded protein isolation. Peptides and their interacting proteins were released by incubation at 50°C for 40 min in RIPA modified buffer. Peptide-interacting proteins were collected and subjected to LC-ESI-MS/MS (HR, medium gradient) protein identification using a mass spectrometer (Orbitrap Exploris 240) and Proteome Discoverer software for analysis (CNB Proteomics Facility, CSIC). Further procedure details are provided as Supplementary material.

Cell transfection and gene reporter assays

Plasmids contained minimal CREB or MEF2 response elements upstream firefly luciferase reporter gene (respectively, pCRE or pMEF2; see details in Table S1). Primary cultures were transfected as detailed in the Supplementary material and incubation proceeded to complete 24

h. For quantitation, 5-7 totally independent experiments were repeated as indicated, each one including technical quadruplicates for every condition.

RNA extraction and qPCR assay

Total RNA was extracted and analyzed as detailed in the Supplementary material. For each independent experiment, we analyzed technical triplicates for every sample and performed a total of 5 completely independent experiments. Data were normalized, for each experiment, with housekeeping genes: neuronal specific enolase (NSE, for genes having neuronal expression) or glyceraldehyde-3-phosphate dehydrogenase (GAPDH, for GFAP, only expressed in glial cells).

Peptide visualization and immunocytochemistry in cultures

Cells grown on coverslips were incubated for 1 h with biotin-conjugated peptides Bio-TMyc or Bio-sTT1$_{Ct}$ (25 μM) or left untreated, and then fixed for 30 min with 4% paraformaldehyde in PBS. After blocking and permeabilization, incubation with Fluorescein Avidin D and immunocytochemistry were as described in the Supplementary material.

Peptide visualization and immunohistochemistry in brain cortex

Vehicle (saline), Bio-TMyc or Bio-TT1$_{Ct}$ (3 nmol/g) were retro-orbitally injected in mice one hour after induction of photothrombotic damage or, alternatively, undamaged animals. In the first case, animals were sacrificed 5 h after damage induction while, the second group was sacrificed 30 min after peptide administration. The details of brain fixation and cryoprotection for peptide visualization and/or immunohistochemistry are provided in the Supplementary material.

Statistical analysis

Except for box and whiskers plots, data are expressed as mean ± standard error of the mean (SEM) of at least four independent experiments. The details of the number of completely independent experiments done (n) and the specific statistical test applied can be found in each respective figure legend. For viability, mRNA and gene reporter assays, technical replicates were included in each independent experiment. Treatment assignation was performed at random.

Statistical analysis was performed in GraphPad Prism 8.0.2. The normality of the data was analyzed by Saphiro-Wilk test. In all cases *P*-value significance is considered as: *$P < 0.05$, ** $P < 0.01$, *** $P < 0.001$, **** $P < 0.0001$. A *P*-value larger than 0.05 is considered non-significant (n.s.).

For the *in vivo* neuroprotection study, the number of required animals was calculated using G*Power 3.1.9.7 software, with a statistical power of 0.8 and an alpha error probability of 0.05.

Results

Identification and targeting of TrkB-T1-specific interactome with a CPP containing the isoform C-ter

TrkB-T1-independent functions might require particular protein interactions established by its highly conserved and isoform-specific C-ter (aa 466-476, Figure 1A) [48], which could be altered by specific biological conditions. This is the case of RhoGDI1, the only TrkB-T1-interacting protein previously identified, released from astrocyte constitutive complexes by BDNF/TrkB-T1-binding [29]. Additional TrkB-T1-specific interactions established in neurons and/or astrocytes and how they might be affected by BDNF-binding or excitotoxicity are presently unknown. Thus, we designed CPP Bio-sTT1$_{Ct}$ containing three elements: 1) a biotin molecule that allows peptide visualization and pull-down of interacting proteins; 2) a HIV-1 Tat short basic domain which allows crossing of BBB and plasma membrane to attached cargoes [49,50] and 3) the isoform-specific sequence (Figure 1A). As a negative control, we used a similar peptide containing unrelated sequences corresponding to c-Myc (Bio-TMyc), which could enter NeuN+ (arrowheads) and NeuN- cells (asterisk) present in mixed primary cultures of rat embryonic cortex (Figure 1Bd-f) but had no effects on neuronal viability in basal or excitotoxic conditions [38,45]. The major cell-subtype in these cultures corresponds to Neu+ neurons which seem to express lower TrkB-T1 levels compared to NeuN- cells also present in the cultures (Figure 1Be), presumably astrocytes. In fact, primary cultures of cortical astrocytes expressed 7-fold higher TrkB-T1 levels than those found in the mixed cultures of neurons and astrocytes employed here (Figure S1). A vesiculated Bio-sTT1$_{Ct}$ distribution was observed in neurons (Figure 1Bg), resembling that of endogenous TrkB-T1 (Figure 1Bb, e). In fact, staining with Fluorescein Avidin D (Figure 1Bg) and the isoform-specific antibody, prepared with the same TrkB-T1 sequence included in Bio-sTT1$_{Ct}$ (Figure 1Bh), suggested that Bio-sTT1$_{Ct}$ and TrkB-T1 mostly colocalized. A CPP subcellular distribution guided by the specific protein sequences contained might explain the differences observed between Bio-MTMyc (Figure 1Bd) and Bio-sTT1$_{Ct}$ (Figure 1Bg) patterns. Next, we confirmed peptide entry into neurons and astrocytes, as suggested by previous experiment, by double staining with cell-type specific markers, respectively NeuN and GFAP (Figure 1C). Bio-sTT1$_{Ct}$ and Bio-TMyc were found inside both NeuN+ (arrowheads) and GFAP+ (asterisks) cells present in the mixed cultures, corresponding respectively to neurons and astrocytes.

Above data suggested that Bio-sTT1$_{Ct}$ might interfere protein interactions established by TrkB-T1 C-ter required, for example, for neuronal death promotion in a context of excitotoxicity.

Accordingly, cell viability was not affected by Bio-TMyc and Bio-sTT1$_{Ct}$ in basal conditions (Figure 1D) while they differently affected the strong and time-dependent decrease in neuronal viability induced by NMDAR overactivation with co-agonists NMDA (100 μM) and glycine (10 μM), herein simply denoted as NMDA (Figure 1E). Preincubation with Bio-sTT1$_{Ct}$ had a significant neuroprotective effect after 2 (50 ± 5%) or 4 h (32 ± 3%) of excitotoxicity compared to Bio-TMyc-treated cultures (respectively, 24 ± 3%, ****$P < 0.0001$ and 16 ± 3%, **$P < 0.01$; $n = 8$).

These results are suggestive of Bio-sTT1$_{Ct}$ being able to interfere protein interactions established by TrkB-T1 inside cells and, thus, this peptide could be used to isolate and identify the isoform specific interactome in different biological conditions. Cultures were incubated with Bio-TMyc or Bio-sTT1$_{Ct}$ (30 min) before treatment with BDNF (100 ng/ml) or NMDA (100 μM) for 30 additional minutes, or left untreated (Figure 2A). Intracellular complexes formed by biotin-labelled peptides were isolated from lysates using streptavidin-agarose precipitation. Then, proteins interacting with Bio-TMyc and Bio-sTT1$_{Ct}$ were identified by a label free proteomic assay, obtaining a total of 4697 proteins for the three different biological conditions and four independent experiments analyzed. Some proteins might be interacting with shared peptide elements such as the biotin moiety or the Tat sequence, or even streptavidin-agarose (Figure 2A). Therefore, we evaluated by a Principal Component Analysis (PCA) whether the interactome profiles obtained were different for both peptides (Figure 2B). The first and second principal components of this analysis (respectively, PC1 and PC2) split the samples into two groups, proving a differential profile of interactions for Bio-TMyc and Bio-sTT1$_{Ct}$.

To emphasize those proteins more specifically interacting with Bio-sTT1$_{Ct}$, we calculated Pearson's correlation between average protein interactions established by Bio-TMyc and Bio-sTT1$_{Ct}$ at the different conditions (Figure 2C-2E). Then, we analyzed the correlation line residuals and selected the top 20% of proteins having higher average interaction with Bio-sTT1$_{Ct}$ compared to Bio-TMyc (highlighted as colored dots). Some of the 453 selected proteins maintained Bio-sTT1$_{Ct}$-interaction at all three conditions while others were affected by BDNF or NMDA treatment (Figure 2F). Interestingly, gene ontology (GO) analysis of biological process enrichment (string.db) associated with Bio-sTT1$_{Ct}$-interacting proteins presented terms related to gene expression and mRNA regulation, including splicing, at all treatment conditions (Figure S2). Only upon NMDA treatment, other biological processes terms appeared such as cytoskeletal reorganization and cell division (Figure S2C).

Then, we further characterized the impact of cell conditions on Bio-sTT1$_{Ct}$ interactions by differential analysis of binding for previously selected proteins (Figure 2G-I). Significant

differences were found in all comparisons (named proteins in corresponding figures, summarized in Table S2), proving that some Bio-sTT1$_{Ct}$-protein complexes were affected by specific stimuli. Thus, BDNF induced Bio-sTT1$_{Ct}$-binding of proteins involved in endocytosis and molecular trafficking (*Gak*), cholesterol metabolism (*CYP46A1*), pre-rRNA processing (*Ftsj3*) or mitochondria-endoplasmic reticulum contact sites (*MERCS*) (*Mtx2*/*Grp75*; Figure 2G). Meanwhile, excitotoxicity promoted significant changes in binding of proteins involved, among others, in gene expression (*Otud6b*, *Ago2*, *Rbm6* and *Ptbp1*; Figure 2I) and cytoskeletal remodeling (*Septin7*, *Pak5*, *Capn5*; Figure 2H-I). Furthermore, comparison of enriched pathways (Reactome, string.db) among tested conditions showed general Bio-sTT1$_{Ct}$-interaction with proteins involved in translation, RNA metabolism and splicing, as seen before in the biological process terms (Figure S2), while BDNF treatment enriched pathways related to vesicle transport and mTOR regulation (Figure 2J). In fact, vesicle transport was also increased with NMDA, while other pathways key for neurotoxicity promotion such as innate immune system, L1CAM interactions, cellular response to stress, axon guidance and RhoGTPases activity specifically appeared. These changes suggest an important role of TrkB-T1 C-ter in excitotoxicity development by interaction with proteins involved in this pathological process.

Next, we analyzed in detail the group of Bio-sTT1$_{Ct}$-interacting proteins included in Reactome function "Signaling by RhoGTPases" (Table S3 and Figure 2K), a pathway enriched after NMDA treatment (Figure 2J). RhoGDI (*Arhgdia* encoded), which is expressed in neuronal-enriched cortical cultures (Figure S3), presented a very low binding to Bio-sTT1$_{Ct}$ and did not pass the established selection criteria, being included in the analysis only as a reference (Figure 2K). This result suggests that TrkB-T1/RhoGDI interaction might be different in neurons and astrocytes [29]. Regarding other RhoGTPase-related proteins (Table S3), most of them presented a very reduced binding after BDNF stimulation while two opposite Bio-sTT1$_{Ct}$-interacting patterns were found in excitotoxicity compared to basal conditions. The interaction was downregulated by NMDA for an important group of proteins, including cytoskeleton components (*Actc1, Tubb2b, Tuba1a, Sptbn1*), Rho and Rac GEFs (respectively *Arhgef12* and *Prex1*) or a Cdc42 effector (*Cdc42bpb*). In contrast, Bio-sTT1$_{Ct}$-interaction was promoted by NMDA for some proteins including *Actr2* and *Arpc3*, components of the Arp2/3 complex mediating actin polymerization, *C1qbp*, involved in inflammation, *Nup98* and *Ranbp2*, components of the nuclear pore complex (NPC) and involved in RNA transport, *Elmo2*, a regulator of Rac GTPase activity and *Pak5*, a downstream effector of Rac1 and Cdc42 GTPases.

Altogether, these results represent a first comprehensive analysis of isoform-specific TrkB-T1 interactions and their modulation in cell models of pathophysiology. Some of the identified TrkB-T1-interacting proteins might contribute to the isoform central role in excitotoxicity and ischemia and help to explain preliminary results showing a neuroprotective effect of Bio-sTT1$_{Ct}$ (Figure 1E), unveiling a new therapeutic strategy to treat stroke and additional excitotoxicity-associated pathologies that merits further investigation.

Design of peptide TT1$_{Ct}$ and mechanism of neuroprotection in cellular models of excitotoxicity

To further characterize the effect of TrkB-T1 interference in excitotoxicity, we designed a new CPP, TT1$_{Ct}$ (Figure 3A). This peptide lacks the biotin molecule, to avoid possible unwanted effects, and contains two spacer prolines separating Tat and isoform-specific sequences, to disrupt a possible regular secondary structure between these functionally-independent moieties that might affect peptide stability and efficacy. As a negative control, we used TMyc, a similar peptide having unrelated c-Myc sequences (Figure 3A) [38,45]. We first analyzed TT1$_{Ct}$ effects on neuronal viability under basal conditions or *in vitro* excitotoxicity (Figure 3B). In a dose-response experiment, TT1$_{Ct}$ resulted toxic for non-stimulated cultures at the higher dose employed (25 μM), probably mimicking some TrkB-T1-ICD neurotoxic effects. In contrast, TT1$_{Ct}$ was not intrinsically toxic at concentrations lower than 25 μM while it was strongly neuroprotective against excitotoxicity. Thus, neuronal viability was 46 ± 7% in cultures preincubated with TT1$_{Ct}$ (15 μM, 30 min) before NMDA treatment (2 h), significantly higher values compared to TMyc-preincubated cells (13 ± 9%, $^{**}P < 0.01$; $n = 8$). Next, in a time-course experiment, we compared the neuroprotective efficacy of TrkB-T1-derived peptides, Bio-sTT1$_{Ct}$ and TT1$_{Ct}$ (15 μM) (Figure 3C), finding similar neuroprotective effects. Neuroprotection due to TT1$_{Ct}$-preincubation was maintained when the peptide was applied at the time of damage induction but lost if added at later times (Figure S4), suggesting that this peptide affects processes taking place in cultures at early times of excitotoxicity.

Our next goal was to investigate the mechanism of TT1$_{Ct}$ neuroprotection. We have previously shown that excitotoxicity induces a progressive increase in TrkB-T1 levels [9] which probably contributes to neuronal death. Other proteins also affected by NMDAR overactivation are TFs CREB and MEF2. Levels of S133 phosphorylated CREB (pCREB), generally considered the active protein, are strongly reduced early upon excitotoxicity induction probably due to phosphatase activation. The result is CREB shut-off, inhibition of BDNF expression and death of mature neurons [51]. In addition, there is a severe MEF2D decrease in cultures subjected to

excitotoxicity [38], probably due to caspases or calpain action [52,53]. The effect of excitotoxicity in cultures incubated with TMyc (15 μM, 30 min) before NMDA treatment (0-120 min) was as expected (Figure 3D-E). At these early times of excitotoxicity, $TT1_{Ct}$ did not have significant effects in TrkB-T1 regulation (Figure 3D) but partially preserved pCREB and MEF2D, although differences were not statistically significant compared to TMyc-treated cultures (Figure 3E). Neuron-specific enolase (NSE), a protein not affected by NMDA, was used as a loading control and for protein normalization. Altogether, these results suggest that one mechanism of $TT1_{Ct}$ neuroprotection might be mediated by CREB and MEF2D through gene expression regulation.

To further explore the potential role of $TT1_{Ct}$ on CREB and MEF2, we performed reporter assays using promoters with minimal response elements (respectively, pMEF2 [54] or pCRE [21]; see Table S1) regulating luciferase expression. In basal conditions, $TT1_{Ct}$ and TMyc (15 μM) had no significant effects on pCRE and pMEF promoter activities compared to untreated cultures (Figure 3F). Excitotoxicity provoked a dramatic decrease in luciferase activity in vehicle or TMyc-preincubated cultures which was significantly prevented by $TT1_{Ct}$. An inactive pMEF mutant with reduced luciferase expression was unresponsive to NMDA or peptide treatment, proving that excitotoxicity regulates MEF2-promoter activity and $TT1_{Ct}$ has a specific effect on it.

Above results are important because these TFs are central to neuronal survival induced by synaptic activity [55,56] or neurotrophins [15,16]. In addition, CREB also regulates the activity of astrocytes in response to neurotransmitters [57-59]. To establish if $TT1_{Ct}$ alters excitotoxicity-induced transcriptional changes in neurons and/or astrocytes, we next analyzed levels of mRNAs encoding proteins involved in survival/death choices (Figure 4). As expected, NMDA induced a strong decrease in levels of mRNAs encoding GluN1 [60], GluN2A [60] and TrkB-FL [9] in TMyc or $TT1_{Ct}$ presence (Figure 4A-C). In contrast, we confirmed a NMDA-induced increase in TrkB-T1 mRNA [60] in TMyc-treated cells, that was counteracted by $TT1_{Ct}$ action (Figure 4D). For BDNF, excitotoxicity showed a tendency to increase mRNA levels in TMyc presence, in agreement to previous results [61], and such accumulation was strongly exacerbated by $TT1_{Ct}$ (Figure 4E). Finally, this peptide decreased GFAP mRNA levels relative to those found in TMyc-treated cultures in excitotoxicity (Figure 4F). In conclusion, $TT1_{Ct}$ does not seem to affect the transcriptional downregulation of the analyzed neuronal genes induced by excitotoxicity while it strongly modifies transcription of genes expressed in astrocytes (GFAP) or both neurons and astrocytes (TrkB-T1 and BDNF), where it counteracts excitotoxic effects. Altogether, we conclude that interference of TrkB-T1 interactions by $TT1_{Ct}$ during

excitotoxicity maintains levels and promoter activities of CREB and MEF2, which regulate the transcription of TrkB-T1 itself and, other target genes critical to neuronal survival and astrocyte activation.

Effects of $TT1_{Ct}$ in a model of ischemic stroke induced by photothrombosis

Our next objective was to investigate if $TT1_{Ct}$ could counteract brain degeneration and interfere TrkB-T1/GFAP expression when excitotoxicity occurs *in vivo*. First, we demonstrated that biotinylated $TT1_{Ct}$ (Bio-$TT1_{Ct}$) and Bio-TMyc (3 nmol/g), intravenously (i.v.) injected into undamaged animals, were able to cross the BBB and efficiently reach most cortical cells in 30 min, being distributed in cell bodies (asterisks) and projections (arrowheads) (Figure S5). Then, we selected a mouse model of permanent ischemia induced by microvascular photothrombosis, which reproduces embolic or thrombotic occlusion of small arteries often produced in human stroke [62]. Photothrombosis causes early breaking of the BBB [63] and damage of cortical motor and somatosensory regions, infarcts being detected after 3 h [38] and reaching maximum volumes by 24 h (Figure 5A). Using confocal microscopy (Figure 5B) or a Cell Observer (Figure S6A), respectively for a detailed analysis or a more general overview, we studied the expression of the TrkB isoforms together with cell-type specific markers in the area of the emerging infarct of animals treated with the control peptide 1 h after damage initiation. We confirmed a strong decrease of TrkB-FL in neurons of the infarcted area, identified by condensed nuclei indicative of cell injury, by 5 h of injury. In contrast, levels of TrkB-T1 and GFAP already increased in the infarcted area at this early time of damage, particularly in the interface of ischemic and non-ischemic tissue which might correspond to the emerging glial scar. Similar results were obtained in animals injected as before with vehicle (Figure S6B). Next, we analyzed Bio-TMyc and Bio-$TT1_{Ct}$ distribution in male and female mice cortex 5 h post-stroke, detecting them in both neuronal (arrows), and non-neuronal cells (asterisks) of the contralateral hemisphere (Figure 5C). Peptide detection at least 4 h after administration suggests a relative stability in brain.

To investigate $TT1_{Ct}$ effects on the glial subpopulation in stroke, we first evaluated GFAP and complement component 3 (C3) co-staining after 5 h (Figure 6A) or 24 h (Figure 6B) of injury. C3 is a marker of inflammatory reactive astrocytes which, among other features, lose the capacity to support neuronal survival and synaptogenesis, and induce death of neurons and mature differentiated oligodendrocytes [7]. TMyc-treated animals had most GFAP+ cells co-stained by the C3 antibody at the infarct boundary, both at 5 and 24 h of damage. Moreover, the number of cells identified as GFAP+/C3+ strongly increased over time. In contrast, early

after injury, $TT1_{Ct}$ caused a strong decrease in GFAP+/C3+ cells. In addition to an early effect on glial scar formation, we investigated a possible $TT1_{Ct}$ impact on macrophage infiltration and microglia activation in injured brain (Figure 6C-G). Protein CD68 (ED1), expressed in macrophages, activated microglia and other cell types, was detected in the infarct border and core of animals treated with TMyc, while it was absent of the contralateral region (Figure 6C). Most CD68+ cells had a rounded morphology compatible with macrophages, although more elongated cells were also detected (Figure 6D). $TT1_{Ct}$ treatment greatly decreased CD68+ cells in the infarct and surrounding tissues, in parallel with reduced immunoglobulin infiltration (Figure S7), produced as early as 2.5 h after injury by BBB damage [45]. Expression of Iba1, a protein present in microglia and circulating macrophages (Figure 6E), was detected in cells with ramified morphology characteristic of resting microglia located in the contralateral region of TMyc and $TT1_{Ct}$-treated animals (Figure 6E-F). Iba1 upregulation was observed in ischemic brain of TMyc-treated animals accompanied by morphological cellular changes indicative of hypertrophic activated microglia. $TT1_{Ct}$ limited Iba1 upregulation in reactive microglia and decreased these cells presence in damaged tissue (Figure 6E). Double immunostaining showed very little CD68/Iba1 signal overlapping (Figure 6G). Altogether, these results show the importance of TrkB-T1 in glial scar formation and inflammatory response after ischemia, as well as the possibility to restrain these processes by using brain-accessible peptide $TT1_{Ct}$.

Finally, we characterized if $TT1_{Ct}$ effects on reactive gliosis resulted in brain protection after ischemic injury and improved the neurological outcome of affected animals. First, we analyzed $TT1_{Ct}$ effect, administered in male and female animals 1 h after damage induction, on infarct volume (Figure 7A) and neurological damage (Figure 7B) evaluated at 24 h. This setting mimics a clinical situation where neuroprotective molecules are provided after insult onset. $TT1_{Ct}$ (3 nmol/g, i.v.) significantly reduced infarct size (10 ± 1% relative to total hemisphere volume) compared to TMyc (17 ± 2%, $***P < 0.001$, $n = 19$; Figure 7A). Notably, $TT1_{Ct}$ administered 10 min after damage had a comparatively modest effect on infarct volume (23%) and neurological damage (29%) (data not shown). Gender disaggregated data showed, for TMyc-treated animals, a tendency to reduced infarct volume in female mice compared to male (15 ± 2% versus 20 ± 1%; $P = 0.08$, $n = 9$: Figure 7C). However, $TT1_{Ct}$-treatment decreased infarct volume to a similar extent, respectively 42% and 45% in female and male mice, peptide differences being statistically significant for both genders ($*P < 0.05$ for female, $**P < 0.01$ for male; Figure 7C). Interestingly, there was a sex-dependent difference in the neurological damage due to ischemia. In male animals, changes in balance and motor coordination established in the beam walking test correlated with injury (Figure 7D). Thus, TMyc-treated

mice presented a significant higher number of slips (10 ± 1) compared to $TT1_{Ct}$-treatment (5 ± 1, ***$P < 0.001$, $n = 12$), representing a 49% recovery. However, TMyc-treated female mice showed more discreet motor deficits than males (5 ± 1 versus 10 ± 1, **$P < 0.01$, $n = 10$), hindering the observation of a $TT1_{Ct}$ effect with this test and suggesting a sexual dimorphism in the neurological outcome after ischemia.

In conclusion, these results demonstrate that peptide $TT1_{Ct}$ is able to rapidly reach the brain cortex of animals with an intact BBB or those subjected to ischemia, where it can be detected in cortical neurons and astrocytes for at least 4 h. As summarized in Figure 7E, this CPP is neuroprotective both in male and female mice subjected to ischemia, reducing infarct size in parallel to neuroinflammation. Furthermore, $TT1_{Ct}$ improves neurological deficits resulting from ischemia in the male subpopulation. Altogether, these data support the importance of protein interactions established by TrkB-T1 C-ter in reactive gliosis after brain damage, a process that has an impact on neurotrophic-signaling and neuronal survival.

Discussion

Glial cells reactivity and subsequent inflammation are processes common to stroke [64] and other neurodegenerative conditions [65,66]. These cells contribute to neurological diseases by protective and detrimental effects implying complex and heterogeneous changes in cell morphology, gene expression and function. Consequently, glial-targeted neuroprotective therapies able to modulate neuroinflammation are a priority. Receptor TrkB-T1, expressed both in neurons and glial cells, is relevant to neuronal excitotoxicity [9,35] while, in astrocytes, promotes injury and oedema formation after stroke [33]. Specific interactions established by TrkB-T1 with still undefined proteins might be important for reactive gliosis and neurotoxicity and, therefore, their modification might prevent such pathological processes and decrease ischemic damage. We have designed brain-accessible peptides containing the TrkB-T1 isoform-specific sequence and show that they modulate reactive gliosis and are strongly neuroprotective against *in vitro* and *in vivo* excitotoxicity.

An important mechanism of $TT1_{Ct}$ action in excitotoxicity is maintenance of CREB/MEF2 activities, essential in neuroinflammation by brain injury [67-69] and neuronal survival/death [51,70]. Compared to neurons, CREB role in astrocytes is not completely defined [71] although different adaptative transcriptional programs are regulated in both cell types [72]. In excitotoxicity, maintenance of CREB/MEF2 promoter activities by $TT1_{Ct}$ action changes levels of CREB and/or MEF2-regulated mRNAs encoding proteins important for astrocyte function. Thus, $TT1_{Ct}$ induces a strong increase of CREB/MEF2-regulated *Bdnf* transcription [18-20]

while it inhibits TrkB-T1 and GFAP expression, suggesting positive and negative effects of these TFs in astrocytes. An inverse association of CREB or MEF2D activation with GFAP expression has been previously described in models of Alzheimer disease [73] or isoflurane neuroprotection in ischemia/reperfusion [74]. These results are relevant because GFAP expression levels, alongside astrocyte reactivity, are considered proportional to injury severity [75].

Similar $TT1_{Ct}$ effects were observed in a preclinical stroke model, where excitotoxicity occurs *in vivo*. Very early after ischemic damage (5 h), proteins TrkB-T1 and GFAP increase in some cells of the infarcted area, particularly in the interface between ischemic and non-ischemic tissue. At later times (24 h), GFAP expression further increases in this area in TMyc-treated animals, mostly in C3+ cells indicative of inflammatory astrocytes. In contrast, $TT1_{Ct}$ strongly decreases GFAP+/C3+ cells at both times. Remarkably, $TT1_{Ct}$ also downregulates macrophage entry and IgG infiltration into the injured tissue, indicative of reduced BBB damage. Finally, microglial Iba1 upregulation in the infarct core and the interface between ischemic and non-ischemic tissue is also decreased by $TT1_{Ct}$ action. Globally, these results demonstrate the importance of signaling mediated by TrkB-T1 C-ter in the modulation of the acute inflammatory response after stroke. Complexes formed by unprocessed TrkB-T1 or RIP TrkB-T1-ICD fragment might regulate the expression of proteins central to ischemia such as the truncated receptor itself, GFAP, C3 or Iba1. This regulation might depend on CREB/MEF2 or additional TFs. One possibility is that, similarly to Notch-ICD [76], TrkB-T1-ICD directly interacts with CREB and alters CREB-dependent expression. Anyway, by interfering TrkB-T1-interactions, $TT1_{Ct}$ might prevent excitotoxicity-induced transcriptional changes, resulting in decreased microglia and astrocyte reactivity after ischemia.

To integrally expose specific TrkB-T1-interacting proteins in different types of neural cells and their relevance in receptor-signaling and function, particularly in the context of an excitotoxic response, we performed proteomic analysis of primary cortical cultures, our *in vitro* model of excitotoxicity. Thus, the identified proteins might correspond to those interacting with TrkB-T1 in neurons, astrocytes or both. In the future, it would be interesting to perform similar studies in primary cortical cultures enriched in astrocytes or neurons. Except for RhoGDI, discovered in astrocyte extracts by affinity chromatography with the isoform-specific peptide [29], no other TrkB-T1-interacting proteins had been previously identified. Results presented here demonstrate that Bio-$sTT1_{Ct}$ establishes a specific protein-interacting profile inside neural cells which is susceptible to different conditions. A differential analysis of Bio-$sTT1_{Ct}$-interactions shows that, independently of treatment, this peptide interacts with proteins highly involved in

gene expression, including RNA modification or splicing, such as the RNA editing enzyme adenosine deaminase acting on RNA (ADAR1). This protein, highly induced in astrocytes after stroke, exacerbates ischemic-injury via astrocyte-mediated neuronal apoptosis [77]. Regarding BDNF treatment, an enrichment of pathways mainly related with vesicle transport and mTOR regulation is observed. Thus, BDNF induces a significant increase in Bio-sTT1$_{Ct}$-binding to neuron-enriched cholesterol 24-hydroxylase (CYP46A1), which controls cholesterol turnover and synthesis of a product that contributes to ischemic damage [78]. Finally, excitotoxicity also produces an enrichment in pathways related with vesicle transport and, more specifically, interrelated pathways involved in axon guidance, innate immune response, including L1CAM interactions, or RhoGTPases-signaling. This protein family, together with RhoGTPase-related proteins, connects activation of surface receptors to cytoskeleton organization, coordinating processes such as cell migration and polarity, cell cycle progression, transcription or neuronal survival/death [30]. RhoGTPases are also central to development of the ischemic damage, particularly in morphological changes associated with reactive gliosis [79].

One protein involved in RhoGTPase-signaling that differentially and significantly interacts with Bio-sTT1$_{Ct}$ in excitotoxicity is p21-activated kinase 5 (PAK5), which belongs to a family of downstream effectors of Rac1/Cdc42 RhoGTPases. PAK proteins participate in cytoskeleton remodeling, promotion of inflammatory cells transcription, and survival [80]. Interestingly, microglia uses a P2Y12R-Rac-PAK-F-actin pathway to alleviate neurons from cytotoxic protein aggregates and regulate delivery of healthy mitochondria to burdened neurons through tunnelling nanotubes (TNTs) [81]. Another protein central to TNT formation is actin-related protein 2/3 (Arp2/3), a multiprotein complex that modulates actin polymerization/depolymerization downstream of Rac. Notably, two Arp2/3 subunits (Actr2/Arp2 and Arpc3/p21-Arc) differentially interact with Bio-sTT1$_{Ct}$ in excitotoxicity. Finally, activation in axons of PAK5 synthesis and signaling after spinal cord injury or cerebral ischemia protects neurons from an axonal energy crisis by reprogramming mitochondrial trafficking and anchoring [82]. Other RhoGTPases-related proteins that differently interact with Bio-sTT1$_{Ct}$ in excitotoxicity are the putative receptor of complement component 1q (C1qbp), C1q being secreted by reactive microglia and involved in induction of neurotoxic reactive astrocytes [7], proteins Nup98 and Ranbp2, important for maintenance and/or assembly of the nuclear pore complex and nucleocytoplasmic transport [83], and engulfment and cell motility 2 (Elmo2) protein, an upstream Rac1 regulator required for phagocytosis and cell migration [84]. Altogether, our results strongly suggest that excitotoxicity might alter specific interactions established by TrkB-T1 with proteins involved in RhoGTPase-signaling, critical to cell

morphology, neuronal survival and reactive gliosis. While some TrkB-T1-interactions are inhibited in excitotoxicity, others are strongly promoted. Displacement by Bio-sTT1$_{Ct}$ of the latter could interfere pathways associated to neuroinflammation and neurotoxicity, thus leading to neuroprotection.

The complexity of TrkB-T1 interactome allows us to propose that a combination of mechanisms affecting neurons and astrocytes alike could be responsible for TT1$_{Ct}$ neuroprotective actions, demonstrated in excitotoxicity *in vitro* and *in vivo*. In cortical cultures, the peptide is strongly neuroprotective when used at moderate concentrations (15 μM) and added before or at the time of the excitotoxic stimulus. This result is important from a preclinical and clinical perspective because, differently from cultured cells, excitotoxicity is not synchronous *in vivo*. By the time treatment is initiated in the ischemia model, penumbra neurons, an important therapeutic target, would be exposed, if not properly protected, to secondary damage associated to infarct expansion. In fact, TT1$_{Ct}$-treatment 1 h after ischemic injury leads to a significant reduction of the infarct volume both in male and female mice, a result particularly relevant considering that our preclinical model has a relatively narrow ischemic penumbra [85]. It will be interesting to analyze in the future if treatment with TT1$_{Ct}$ can be delayed further after damage. Interestingly, results obtained in male and female mice reveal a sexual dimorphism relative to the effect of the ischemic damage on motor coordination and balance. As previously described [38,45], males show pronounced deficits which can be improved by TT1$_{Ct}$, while females are less compromised despite having similar infarct volumes. Sexual dimorphism after CNS injury has been previously observed in other studies [86,87], and has been related to a neuroprotective estrogen effect or a decreased neuroinflammatory response in female mice [88]. Therefore, future studies on the pathophysiology of ischemic brain damage and testing of therapeutic compounds need to consider the impact of biological sex.

Clinical translation of above results could be limited by a predictable low plasma stability of TT1$_{Ct}$, conditioning peptide brain bioavailability and efficacy. However, as previously described in patients treated with nerinetide, a low CPP half-life is not necessarily related to a lack of neuroprotection. Nerinetide is a Tat-derived CPP (20 aa) that dissociates the ternary complex formed by NMDAR-GluN2B subunits with scaffold protein PSD-95 and neuronal nitric oxide synthase (nNOS) [89]. In an excitotoxic context, this peptide reduces nNOS activation, nitric oxide (NO) production and oxidative damage, resulting in neuroprotection in different preclinical stroke models [89-91]. Remarkably, in the course of a phase 3 clinical trial for acute ischemic stroke, nerinetide-treatment had a clinical benefit in patients undergoing endovascular therapy without concurrent or previous thrombolytic treatment, even when the

plasma half-life of nerinetide was below 20 min [42]. One possibility is that CPP stability once it reaches the brain tissue is higher compared to plasma, as suggested by our results showing the presence of Bio-TMyc and Bio-$TT1_{Ct}$ in male and female brain cortex at least 4 h after administration. Another relevant issue concerning clinical translation is the appropriate time of CPP treatment after onset of stroke symptoms. Recently published results from the FRONTIER clinical assay (NCT0231544) have shown that administration of nerinetide by paramedics before hospital arrival might benefit patients with acute ischemic stroke as an adjunct to reperfusion therapies if applied within 3 h of symptoms onset [43]. In fact, in this trial, nerinetide treatment of suspected stroke began a median of 64 min (IQR 47-100) from symptoms onset. Furthermore, a *post-hoc* metanalysis of data collected from three completed randomized nerinetide trials enrolling patients up to 12 h after stroke onset further supports the importance of early peptide treatment followed by reperfusion to obtain a clinically significant benefit over several outcome measures [92].

The peptide $TT1_{Ct}$ described in this work has multimodal effects in the damaged brain, affecting neurons as well as glial cells, and might be relevant for the design of novel therapies for human stroke and many other neurological conditions associated with excitotoxicity and neuroinflammation.

Abbreviations

Arp2/3: actin-related protein 2/3; BBB: blood–brain barrier (BBB); BDNF: brain-derived neurotrophic factor; C1q: complement component 1q; C3: complement component 3; CPP: cell-penetrating peptide; CREB: cAMP response element-binding protein; CYP46A1: cholesterol 24-hydroxylase; DIVs: days *in vitro*; Elmo2: engulfment and cell motility 2 protein; GABA: gamma aminobutyric acid; GAPDH: glyceraldehyde-3-phosphate dehydrogenase; GFAP: glial fibrillary acidic protein; GO: gene ontology; ICDs: intracellular domains; MEF2: myocyte enhancer factor 2; MPs: metalloproteinases; NDDs: neurodegenerative diseases; NMDARs: N-methyl-D-aspartate receptors; NPC: nuclear pore complex; n.s.: non-significant; NSE: neuronal specific enolase; PAK5: p21-activated kinase 5; PCA: Principal Component Analysis; RhoGDI1: RhoGDP dissociation inhibitor 1; RIP: regulated intermembrane proteolysis; TFs: transcription factors; TK: tyrosine kinase; TNTs: tunnelling nanotubes; TrkB: tropomyosin-related kinase B receptor; TrkB-FL: full-length TrkB.

Data availability

The data that support the findings of the proteomic study are available from the corresponding author, upon reasonable request.

Acknowledgements

We acknowledge funding from Agencia Estatal de Investigación (PID2019-105784RB-100/AEI/10.13039/501100011033/FEDER, UE). These results are also part of project PID2022-137710OB-I00 funded by MICIU/AEI/10.13039/501100011033/FEDER, UE. The cost of publication has been paid in part by FEDER funds. A contract was funded associated to project PID2019-105784RB-100 (G.M.E-O) and L.U-T. was recipient of fellowships from Spanish Ministry of Universities "Ayuda del Programa de Formación de Profesorado Universitario" with code FPU22/01248 (2024-2028) and "Ayuda para el Fomento de la Investigación en Estudios de Master-UAM" fellowship from Universidad Autónoma de Madrid (2021-2022). We are grateful to Drs. Gutiérrez (IdiPaz, HU La Paz), Lorrio (UAM), Sobrado (HU La Princesa), Avendaño and Negredo (Departamento de Anatomía, Histología y Neurociencia, UAM, Spain) for technical advice with the ischemia model. We also thank "Conexión de Namomedicine" from CSIC for their support. We acknowledge the contribution of Genomics and Microscopy Core Units (IIBM, CSIC) as well as the Proteomics Core Facility at Centro Nacional de Biotecnología (CNB, CSIC). Finally, we also thank Dr. M.C. Serrano (Instituto de Ciencia de Materiales de Madrid, CSIC) and members of our group for helpful discussions.

Competing interests

The authors report no competing interests.

References

1. DeLong JH, Ohashi SN, O'Connor KC, Sansing LH. Inflammatory responses after ischemic stroke. Semin Immunopathol. 2022; 44: 625-48.

2. Shen XY, Gao ZK, Han Y, Yuan M, Guo YS, Bi X. Activation and role of astrocytes in ischemic stroke. Front Cell Neurosci. 2021; 15: 755955.

3. Escartin C, Galea E, Lakatos A, O'Callaghan JP, Petzold GC, Serrano-Pozo A, et al. Reactive astrocyte nomenclature, definitions, and future directions. Nat Neurosci. 2021; 24: 312-25.

4. Hasel P, Rose IVL, Sadick JS, Kim RD, Liddelow SA. Neuroinflammatory astrocyte subtypes in the mouse brain. Nat Neurosci. 2021; 24: 1475-87.

5. Verkhratsky A, Parpura V, Li B, Scuderi C. Astrocytes: the housekeepers and guardians of the CNS. Adv Neurobiol. 2021; 26: 21-53.

6. Cserep C, Posfai B, Lenart N, Fekete R, Laszlo ZI, Lele Z, et al. Microglia monitor and protect neuronal function through specialized somatic purinergic junctions. Science. 2020; 367: 528-37.

7. Liddelow SA, Guttenplan KA, Clarke LE, Bennett FC, Bohlen CJ, Schirmer L, et al. Neurotoxic reactive astrocytes are induced by activated microglia. Nature. 2017; 541: 481-7.

8. Prabhakaran S, Ruff I, Bernstein RA. Acute stroke intervention: a systematic review. JAMA. 2015; 313: 1451-62.

9. Vidaurre OG, Gascón S, Deogracias R, Sobrado M, Cuadrado E, Montaner J, et al. Imbalance of neurotrophin receptor isoforms TrkB-FL/TrkB-T1 induces neuronal death in excitotoxicity. Cell Death & Dis. 2012;3:e256.

10. Tejeda GS, Diaz-Guerra M. Integral characterization of defective BDNF/TrkB signalling in neurological and psychiatric disorders leads the way to new therapies. Int J Mol Sci. 2017;18:268.

11. Riley CP, Cope TC, Buck CR. CNS neurotrophins are biologically active and expressed by multiple cell types. J Mol His. 2004; 35: 771-83.

12. Lei L, Parada LF. Transcriptional regulation of Trk family neurotrophin receptors. Cell Mol Life Sci. 2007; 64: 522-32.

13. Middlemas DS, Lindberg RA, Hunter T. trkB, a neural receptor protein-tyrosine kinase: evidence for a full-length and two truncated receptors. Mol Cell Biol. 1991; 11: 143-53.

14. Niu C, Yue X, An JJ, Bass R, Xu H, Xu B. Genetic Dissection of BDNF and TrkB Expression in Glial Cells. Biomolecules. 2024; 14: 91.

15. Bonni A, Brunet A, West AE, Datta SR, Takasu MA, Greenberg ME. Cell survival promoted by the Ras-MAPK signaling pathway by transcription-dependent and -independent mechanisms. Science. 1999; 286: 1358-62.

16. Liu L, Cavanaugh JE, Wang Y, Sakagami H, Mao Z, Xia Z. ERK5 activation of MEF2-mediated gene expression plays a critical role in BDNF-promoted survival of developing but not mature cortical neurons. Proc Natl Acad Sci U S A. 2003; 100: 8532-7.

17. Wang Y, Liu L, Xia Z. Brain-derived neurotrophic factor stimulates the transcriptional and neuroprotective activity of myocyte-enhancer factor 2C through an ERK1/2-RSK2 signaling cascade. J Neurochem. 2007; 102: 957-66.

18. Lyons MR, Schwarz CM, West AE. Members of the myocyte enhancer factor 2 transcription factor family differentially regulate Bdnf transcription in response to neuronal depolarization. J Neurosci. 2012; 32: 12780-5.

19. Shieh PB, Hu SC, Bobb K, Timmusk T, Ghosh A. Identification of a signaling pathway involved in calcium regulation of BDNF expression. Neuron. 1998; 20: 727-40.

20. Tao X, Finkbeiner S, Arnold DB, Shaywitz AJ, Greenberg ME. Ca2+ influx regulates BDNF transcription by a CREB family transcription factor-dependent mechanism. Neuron. 1998; 20: 709-26.

21. Deogracias R, Espliguero G, Iglesias T, Rodriguez-Pena A. Expression of the neurotrophin receptor trkB is regulated by the cAMP/CREB pathway in neurons. Mol Cell Neurosci. 2004; 26: 470-80.

22. Lau GC, Saha S, Faris R, Russek SJ. Up-regulation of NMDAR1 subunit gene expression in cortical neurons via a PKA-dependent pathway. J Neurochem. 2004; 88: 564-75.

23. Biffo S, Offenhauser N, Carter BD, Barde YA. Selective binding and internalisation by truncated receptors restrict the availability of BDNF during development. Development. 1995; 121: 2461-70.

24. Alderson RF, Curtis R, Alterman AL, Lindsay RM, DiStefano PS. Truncated TrkB mediates the endocytosis and release of BDNF and neurotrophin-4/5 by rat astrocytes and schwann cells in vitro. Brain Res. 2000; 871: 210-22.

25. Rose CR, Blum R, Pichler B, Lepier A, Kafitz KW, Konnerth A. Truncated TrkB-T1 mediates neurotrophin-evoked calcium signalling in glia cells. Nature. 2003; 426: 74-8.

26. Aroeira RI, Sebastiao AM, Valente CA. BDNF, via truncated TrkB receptor, modulates GlyT1 and GlyT2 in astrocytes. Glia. 2015; 63: 2181-97.

27. Vaz SH, Jorgensen TN, Cristovao-Ferreira S, Duflot S, Ribeiro JA, Gether U, et al. Brain-derived neurotrophic factor (BDNF) enhances GABA transport by modulating the trafficking of GABA transporter-1 (GAT-1) from the plasma membrane of rat cortical astrocytes. J Biol Chem. 2011; 286: 40464-76.

28. Holt LM, Hernandez RD, Pacheco NL, Torres Ceja B, Hossain M, Olsen ML. Astrocyte morphogenesis is dependent on BDNF signaling via astrocytic TrkB.T1. Elife. 2019; 8: e44667.

29. Ohira K, Kumanogoh H, Sahara Y, Homma KJ, Hirai H, Nakamura S, et al. A truncated tropomyosin-related kinase B receptor, T1, regulates glial cell morphology via Rho GDP dissociation inhibitor 1. J Neurosci. 2005; 25: 1343-53.

30. Stankiewicz TR, Linseman DA. Rho family GTPases: key players in neuronal development, neuronal survival, and neurodegeneration. Frontiers in cellular neuroscience. 2014; 8: 314.

31. Cao T, Matyas JJ, Renn CL, Faden AI, Dorsey SG, Wu J. Function and Mechanisms of Truncated BDNF Receptor TrkB.T1 in Neuropathic Pain. Cells. 2020; 9: 1194.

32. Ferrer I, Krupinski J, Goutan E, Marti E, Ambrosio S, Arenas E. Brain-derived neurotrophic factor reduces cortical cell death by ischemia after middle cerebral artery occlusion in the rat. Acta Neuropathol. 2001; 101: 229-38.

33. Colombo E, Bacigaluppi M, Bartoccetti M, Triolo D, Bassani C, Bergamaschi A, et al. Astrocyte TrkB promotes brain injury and edema formation in ischemic stroke. Neurobiol Dis. 2024; 201: 106670.

34. Choi DW. Glutamate neurotoxicity and diseases of the nervous system. Neuron. 1988; 1: 623-34.

35. Gomes JR, Costa JT, Melo CV, Felizzi F, Monteiro P, Pinto MJ, et al. Excitotoxicity downregulates TrkB.FL signaling and upregulates the neuroprotective truncated TrkB receptors in cultured hippocampal and striatal neurons. J Neurosci. 2012; 32: 4610-22.

36. Tejeda GS, Ayuso-Dolado S, Arbeteta R, Esteban-Ortega GM, Vidaurre OG, Diaz-Guerra M. Brain ischaemia induces shedding of a BDNF-scavenger ectodomain from TrkB receptors by excitotoxicity activation of metalloproteinases and gamma-secretases. J Pathol. 2016; 238: 627-40.

37. Lee YJ, Ch'ng TH. RIP at the Synapse and the Role of Intracellular Domains in Neurons. Neuromolecular Med. 2020; 22: 1-24.

38. Tejeda GS, Esteban-Ortega GM, San Antonio E, Vidaurre OG, Díaz-Guerra M. Prevention of excitotoxicity-induced processing of BDNF receptor TrkB-FL leads to stroke neuroprotection. EMBO Mol Med. 2019; 11:e9950.

39. Esteban-Ortega GM, Díaz-Guerra M. Retrograde transport of neurotrophin receptor TrkB-FL induced by excitotoxicity regulates Golgi stability and is a target for stroke neuroprotection. bioRxiv. 2024; doi:10.1101/2024.10.29.620835.

40. Varnamkhasti BS, Jafari S, Taghavi F, Alaei L, Izadi Z, Lotfabadi A, et al. Cell-Penetrating peptides: as a promising theranostics strategy to circumvent the blood-brain barrier for CNS diseases. Curr Drug Deliv. 2020; 17: 375-86.

41. Pirhaghi M, Mamashli F, Moosavi-Movahedi F, Arghavani P, Amiri A, Davaeil B, et al. Cell-penetrating peptides: promising therapeutics and drug-delivery systems for neurodegenerative diseases. Mol Pharm. 2024; 21: 2097-117.

42. Hill MD, Goyal M, Menon BK, Nogueira RG, McTaggart RA, Demchuk AM, et al. Efficacy and safety of nerinetide for the treatment of acute ischaemic stroke (ESCAPE-NA1): a multicentre, double-blind, randomised controlled trial. Lancet. 2020; 395: 878-87.

43. Christenson J, Hill MD, Swartz RH, Adams C, Benavente O, Casaubon LK, et al. Efficacy and safety of intravenous nerinetide initiated by paramedics in the field for acute cerebral ischaemia within 3 h of symptom onset (FRONTIER): a phase 2, multicentre, randomised, double-blind, placebo-controlled study. Lancet. 2025; 405: 571-82.

44. Schroeter M, Jander S, Stoll G. Non-invasive induction of focal cerebral ischemia in mice by photothrombosis of cortical microvessels: characterization of inflammatory responses. J Neurosci Methods. 2002; 117: 43-9.

45. Ayuso-Dolado S, Esteban-Ortega GM, Vidaurre OG, Diaz-Guerra M. A novel cell-penetrating peptide targeting calpain-cleavage of PSD-95 induced by excitotoxicity improves neurological outcome after stroke. Theranostics. 2021; 11: 6746-65.

46. Choi DW. Glutamate neurotoxicity in cortical cell culture is calcium dependent. Neurosci Lett. 1985; 58: 293-7.

47. Choi DW, Maulucci-Gedde M, Kriegstein AR. Glutamate neurotoxicity in cortical cell culture. J Neurosci. 1987; 7: 357-68.

48. Tessarollo L, Yanpallewar S. TrkB truncated isoform receptors as transducers and determinants of BDNF functions. Front Neurosci. 2022; 16: 847572.

49. Milletti F. Cell-penetrating peptides: classes, origin, and current landscape. Drug Discov Today. 2012; 17: 850-60.

50. Regberg J, Eriksson JN, Langel U. Cell-penetrating peptides: from cell cultures to in vivo applications. Front Biosci (Elite edition). 2013; 5: 509-16.

51. Hardingham GE, Fukunaga Y, Bading H. Extrasynaptic NMDARs oppose synaptic NMDARs by triggering CREB shut-off and cell death pathways. Nat Neurosci. 2002; 5: 405-14.

52. Tang X, Wang X, Gong X, Tong M, Park D, Xia Z, et al. Cyclin-dependent kinase 5 mediates neurotoxin-induced degradation of the transcription factor myocyte enhancer factor 2. J Neurosci. 2005; 25: 4823-34.

53. Wei G, Yin Y, Li W, Bito H, She H, Mao Z. Calpain-mediated degradation of myocyte enhancer factor 2D contributes to excitotoxicity by activation of extrasynaptic N-methyl-D-aspartate receptors. J Biol Chem. 2012; 287: 5797-805.

54. Woronicz JD, Lina A, Calnan BJ, Szychowski S, Cheng L, Winoto A. Regulation of the Nur77 orphan steroid receptor in activation-induced apoptosis. Mol Cell Biol. 1995; 15: 6364-76.

55. Lonze BE, Ginty DD. Function and regulation of CREB family transcription factors in the nervous system. Neuron. 2002; 35: 605-23.

56. Linseman DA, Bartley CM, Le SS, Laessig TA, Bouchard RJ, Meintzer MK, et al. Inactivation of the myocyte enhancer factor-2 repressor histone deacetylase-5 by endogenous Ca(2+)/calmodulin-dependent kinase II promotes depolarization-mediated cerebellar granule neuron survival. J Biol Chem. 2003; 278: 41472-81.

57. Carriba P, Pardo L, Parra-Damas A, Lichtenstein MP, Saura CA, Pujol A, et al. ATP and noradrenaline activate CREB in astrocytes via noncanonical Ca(2+) and cyclic AMP independent pathways. Glia. 2012; 60: 1330-44.

58. Karki P, Webb A, Smith K, Lee K, Son DS, Aschner M, et al. cAMP response element-binding protein (CREB) and nuclear factor kappaB mediate the tamoxifen-induced up-regulation of glutamate transporter 1 (GLT-1) in rat astrocytes. J Biol Chem. 2013; 288: 28975-86.

59. Modi KK, Jana M, Mondal S, Pahan K. Sodium benzoate, a metabolite of cinnamon and a food additive, upregulates ciliary neurotrophic factor in astrocytes and oligodendrocytes. Neurochem Res. 2015; 40: 2333-47.

60. Gascon S, Deogracias R, Sobrado M, Roda JM, Renart J, Rodriguez-Pena A, et al. Transcription of the NR1 subunit of the N-methyl-D-aspartate receptor is down-regulated by excitotoxic stimulation and cerebral ischemia. J Biol Chem. 2005; 280: 35018-27.

61. Zafra F, Castrén E, Thoenen H, Lindholm D. Interplay between glutamate and gamma-aminobutyric acid transmitter systems in the physiological regulation of brain-derived neurotrophic factor and nerve growth factor synthesis in hippocampal neurons. Proc Natl Acad Sci U S A. 1991; 88: 10037-41.

62. Pevsner PH, Eichenbaum JW, Miller DC, Pivawer G, Eichenbaum KD, Stern A, et al. A photothrombotic model of small early ischemic infarcts in the rat brain with histologic and MRI correlation. J Pharmacol Toxicol Methods. 2001; 45: 227-33.

63. Abdullahi W, Tripathi D, Ronaldson PT. Blood-brain barrier dysfunction in ischemic stroke: targeting tight junctions and transporters for vascular protection. Am J Physiol Cell Physiol. 2018; 315: C343-C56.

64. Xu S, Lu J, Shao A, Zhang JH, Zhang J. Glial Cells: Role of the Immune Response in Ischemic Stroke. Front Immunol. 2020; 11: 294.

65. Paolicelli RC, Sierra A, Stevens B, Tremblay ME, Aguzzi A, Ajami B, et al. Microglia states and nomenclature: A field at its crossroads. Neuron. 2022; 110: 3458-83.

66. Verkhratsky A, Butt A, Li B, Illes P, Zorec R, Semyanov A, et al. Astrocytes in human central nervous system diseases: a frontier for new therapies. Signal Transduct Target Ther. 2023; 8: 396.

67. Yi JH, Park SW, Kapadia R, Vemuganti R. Role of transcription factors in mediating post-ischemic cerebral inflammation and brain damage. Neurochem Int. 2007; 50: 1014-27.

68. Yamaguchi A, Jitsuishi T, Hozumi T, Iwanami J, Kitajo K, Yamaguchi H, et al. Temporal expression profiling of DAMPs-related genes revealed the biphasic post-ischemic inflammation in the experimental stroke model. Mol Brain. 2020; 13: 57.

69. Wu J, Guo Y, Li W, Zhang Z, Li X, Zhang Q, et al. Microglial priming induced by loss of Mef2C contributes to postoperative cognitive dysfunction in aged mice. Exp Neurol. 2023; 365: 114385.

70. Lisek M, Przybyszewski O, Zylinska L, Guo F, Boczek T. The role of MEF2 transcription factor family in neuronal survival and degeneration. Int J Mol Sci. 2023; 24: 3120.

71. Kim J, Kaang BK. Cyclic AMP response element-binding protein (CREB) transcription factor in astrocytic synaptic communication. Front Synaptic Neurosci. 2022; 14: 1059918.

72. Pardo L, Valor LM, Eraso-Pichot A, Barco A, Golbano A, Hardingham GE, et al. CREB regulates distinct adaptive transcriptional programs in astrocytes and neurons. Sci Rep. 2017; 7: 6390.

73. Pugazhenthi S, Wang M, Pham S, Sze CI, Eckman CB. Downregulation of CREB expression in Alzheimer's brain and in Abeta-treated rat hippocampal neurons. Mol Neurodegener. 2011; 6: 60.

74. Zhang Q, Yin J, Xu F, Zhai J, Yin J, Ge M, et al. Isoflurane post-conditioning contributes to anti-apoptotic effect after cerebral ischaemia in rats through the ERK5/MEF2D signaling pathway. J Cell Mol Med. 2021; 25: 3803-15.

75. Escartin C, Guillemaud O, Carrillo-de Sauvage MA. Questions and (some) answers on reactive astrocytes. Glia. 2019; 67: 2221-47.

76. Hallaq R, Volpicelli F, Cuchillo-Ibanez I, Hooper C, Mizuno K, Uwanogho D, et al. The Notch intracellular domain represses CRE-dependent transcription. Cell Signal. 2015; 27: 621-9.

77. Cai D, Fraunfelder M, Fujise K, Chen SY. ADAR1 exacerbates ischemic brain injury via astrocyte-mediated neuron apoptosis. Redox Biol. 2023; 67: 102903.

78. Sun H, Yang T, Simon RP, Xiong ZG, Leng T. Role of Cholesterol Metabolic Enzyme CYP46A1 and Its Metabolite 24S-Hydroxycholesterol in Ischemic Stroke. Stroke. 2024; 55: 2492-501.

79. Lu W, Chen Z, Wen J. The role of RhoA/ROCK pathway in the ischemic stroke-induced neuroinflammation. Biomed Pharmacother. 2023; 165: 115141.

80. Civiero L, Greggio E. PAKs in the brain: Function and dysfunction. Biochim Biophys Acta Mol Basis Dis. 2018; 1864: 444-53.

81. Scheiblich H, Eikens F, Wischhof L, Opitz S, Jungling K, Cserep C, et al. Microglia rescue neurons from aggregate-induced neuronal dysfunction and death through tunneling nanotubes. Neuron. 2024; 112: 3106-25 e8.

82. Huang N, Li S, Xie Y, Han Q, Xu XM, Sheng ZH. Reprogramming an energetic AKT-PAK5 axis boosts axon energy supply and facilitates neuron survival and regeneration after injury and ischemia. Curr Biol. 2021; 31: 3098-114 e7.

83. Ferreira PA. Nucleocytoplasmic transport at the crossroads of proteostasis, neurodegeneration and neuroprotection. FEBS Lett. 2023; 597: 2567-89.

84. Gumienny TL, Brugnera E, Tosello-Trampont AC, Kinchen JM, Haney LB, Nishiwaki K, et al. CED-12/ELMO, a novel member of the CrkII/Dock180/Rac pathway, is required for phagocytosis and cell migration. Cell. 2001; 107: 27-41.

85. Carmichael ST. Rodent models of focal stroke: size, mechanism, and purpose. NeuroRx. 2005; 2: 396-409.

86. Abbasian M, Langlois A, Gibon J. Sexual dimorphism in balance and coordination in p75NTR(exonIII) knock-out mice. Front Behav Neurosci. 2022; 16: 842552.

87. Farooque M, Suo Z, Arnold PM, Wulser MJ, Chou CT, Vancura RW, et al. Gender-related differences in recovery of locomotor function after spinal cord injury in mice. Spinal Cord. 2006; 44: 182-7.

88. Li Y, Ritzel RM, Lei Z, Cao T, He J, Faden AI, et al. Sexual dimorphism in neurological function after SCI is associated with disrupted neuroinflammation in both injured spinal cord and brain. Brain Behav Immun. 2022; 101: 1-22.

89. Aarts M, Liu Y, Liu L, Besshoh S, Arundine M, Gurd JW, et al. Treatment of ischemic brain damage by perturbing NMDA receptor- PSD-95 protein interactions. Science. 2002; 298: 846-50.

90. Teves LM, Cui H, Tymianski M. Efficacy of the PSD95 inhibitor Tat-NR2B9c in mice requires dose translation between species. J Cereb Blood Flow Metab. 2016; 36: 555-61.

91. Cook DJ, Teves L, Tymianski M. Treatment of stroke with a PSD-95 inhibitor in the gyrencephalic primate brain. Nature. 2012; 483: 213-7.

92. Tymianski M, Hill MD, Goyal M, Christenson J, Menon BK, Swartz RH, et al. Safety and efficacy of nerinetide in patients with acute ischaemic stroke enrolled in the early window: a post-hoc meta-analysis of individual patient data from three randomised trials. Lancet Neurol. 2025; 24: 208-17.

Figure legends

Figure 1. Validation of isoform-specific CPPs as tools for identification of TrkB-T1 interactome and prevention of neuronal death by excitotoxicity. (A) Structure of TrkB-T1 receptor, indicating the extracellular domain (ECD), responsible of brain derived neurotrophic factor (BDNF)-binding, the transmembrane segment (TM) and the short intracellular domain (ICD). The precise sequence corresponding to the TrkB-T1 C-ter (dotted oval) is indicated. It contains a region shared with TrkB-FL (black and green) followed by the TrkB-T1-specific sequence (pink). Biotin (Bio)-labelled Tat-derived CPPs, containing this isoform-specific sequence (Bio-sTT1$_{Ct}$) or unrelated sequences for the control peptide (Bio-TMyc), are also indicated. (B) Immunocytochemistry assays of primary cortical cultures treated with Bio-sTT1$_{Ct}$, Bio-TMyc (25 µM) or vehicle for 30 min. TrkB-T1 and Bio-sTT1$_{Ct}$ distribution were analyzed with an isoform specific antibody (red). Peptide visualization with Fluorescein Avidin D (green) shows that Bio-sTT1$_{Ct}$ presents a pattern similar to that observed for endogenous TrkB-T1. Bio-TMyc distribution was visualized in Neu+ (arrowheads) and Neu- (asterisk), corresponding respectively to neurons and presumably astrocytes (d-f). Scale bar, 10 µm. (C) Analysis of cultures treated as before with specific antibodies for astrocytes (GFAP, red) or neurons (NeuN, magenta). Peptide visualization with Fluorescein Avidin D (green) shows distribution in both Neu+ neurons (arrowheads) and GFAP+ astrocytes (asterisk). Scale bar, 10 µm. (D) Cell viability of cortical cultures treated with Bio-sTT1$_{Ct}$ and Bio-TMyc (25 µM) for 4, 6 or 24 h. Means ± SEM and individual points are presented relative to values obtained for 4 h of Bio-TMyc treatment (100%). Data were analyzed using two-way ANOVA test followed by *post hoc* Bonferroni test, $n = 4$. (E) Neuronal viability in cultures incubated with Bio-TMyc or Bio-sTT1$_{Ct}$ (25 µM) for 30 min and treated with NMDA for 2 or 4 h. Means ± SEM and individual points are presented relative to the values obtained for untreated cells (100%). Data were analyzed using two-way ANOVA test followed by *post hoc* Bonferroni test, $n = 8$.

Figure 2. Bio-sTT1$_{Ct}$ as a tool to approach TrkB-T1 specific interactome in different biological conditions. (A) Experimental design of pull-down assays to isolate Bio-TMyc and Bio-sTT1$_{Ct}$ interacting proteins. Cultures were incubated with Bio-sTT1$_{Ct}$ or Bio-TMyc (25 µM) for 30 min before treatment with BDNF (100 ng/ml) or NMDA for 30 min. After that, cell lysates were combined with streptavidin agarose beads to isolate the CPP-interacting proteins. (B) Principal Component Analysis of Bio-TMyc and Bio-sTT1$_{Ct}$ pull-down isolates. Samples are represented using the first (PC1) and second (PC2) components of the analysis. (C-E) Pearson's correlation of the average protein interactions established by Bio-TMyc and Bio-

sTT1$_{Ct}$ in basal conditions (C), or after BDNF (D) or NMDA treatment (E). Colored points represent the top 20% proteins whose residuals are furthest from the correlation line and have higher levels of binding to Bio-sTT1$_{Ct}$. (F) Venn diagram representing the number of proteins selected for each condition following the criteria described above. (G-H) Volcano plot presenting the results of the differential analysis of interacting proteins comparing BDNF vs basal conditions (G), NMDA vs BDNF (H) and NMDA vs basal conditions (I). Log_2FC and -Log_{10}(p-value) are shown. Proteins selected with the criteria explained above are represented as dark grey points while proteins showing statistically significant differences are labelled and presented as brown dots (p-value < 0.05). FDR = 9.52% (G), 4.15% (H) or 9.55% (I). FC, fold change. (I) Pathway enrichment analysis of selected proteins for basal, BDNF and NMDA conditions. A heatmap showing the enrichment score for each pathway (Reactome.db) at the different conditions is presented. (J) Comparison of RhoGDI (*Arhgdia*) (highlighted) and our selected proteins annotated in "Signaling by Rho GTPases" Reactome pathway in basal, BDNF and NMDA conditions. A heatmap showing the z-score indicating levels for each protein at the different conditions is presented.

Figure 3. TrkB-T1-derived peptide TT1$_{Ct}$ is neuroprotective against *in vitro* excitotoxicity and prevents a decrease in CRE and MEF promoter activities induced by the excitotoxic injury. (A) Sequence of control peptide (TMyc) and TrkB-T1-derived CPP (TT1$_{Ct}$). (B) Neuronal viability in cultures incubated with TMyc or TT1$_{Ct}$ (5, 15 or 25 µM) for 30 min and then treated with NMDA (100 µM) for 2 h or left untreated. Individual data and means ± SEM are presented relative to values obtained in the untreated cells (100%). Data were analyzed using Kruskal-Wallis test followed by Mann-Whitney U-test, *n* = 6-16. (C) Neuronal viability in cultures incubated with Bio-TMyc, Bio-sTT1$_{Ct}$ or TT1$_{Ct}$ (15 µM) for 30 min and then treated with NMDA (100 µM) for 2 or 4 h. Individual data and means ± SEM are presented relative to values obtained for untreated cells (100%). Data were analyzed using two-way ANOVA test followed by *post hoc* Bonferroni test, *n* = 6-8. (D) Western Blot analysis of TrkB-T1, pCREB and MEF2D levels in cultures incubated with TMyc or TT1$_{Ct}$ (15 µM) for 30 min followed by treatment for 30, 60 or 120 min with NMDA. A representative experiment is shown. (E) Quantitation by densitometric analysis of pCREB and MEF2D levels. Means ± SEM are presented relative to basal conditions in the presence of TMyc (100%), *n* = 5. (F) Effect of excitotoxicity and TT1$_{Ct}$ treatment on CRE and MEF2 promoter activity. Cultures transfected with plasmids containing minimal CREB or MEF2 response elements (respectively, pCRE and pMEF) or pMEFmut were preincubated with peptides as above and treated with NMDA for 2

h or left untreated. Individual results and means ± SEM are presented relative to luciferase expression in untreated cultures. Data was analyzed by two-way ANOVA test followed by *post hoc* Bonferroni test, n = 5-7. For cultures transfected with pCRE and pMEF, treated with vehicle or TMyc, differences between -/+ NMDA are statistically significant although not shown for simplicity.

Figure 4. $TT1_{Ct}$ interferes transcriptional changes induced by excitotoxicity affecting expression of genes involved in survival/death choices. Cultures preincubated with $TT1_{Ct}$ or TMyc (15 μM) for 30 min were treated with NMDA for 4 h or left untreated. Levels of mRNAs encoding for NMDAR-subunits GluN1 (A) and GluN2A (B) or TrkB-FL (C) and TrkB-T1 isoforms (D) were normalized to those of NSE. Levels of BDNF (E) and GFAP mRNA (F) were normalized relative to GAPDH. Individual values and means ± SEM are presented relative to gene expression in cultures treated with TMyc (100%). Data were analyzed by two-way ANOVA test followed by *post hoc* Tukey's or Kruskal Wallis test followed by *post hoc* Dunn's test, n = 5.

Figure 5. $TT1_{Ct}$ brain distribution in a mouse model of permanent ischemia showing upregulation of TrkB-T1+/GFAP+ cells in the interface between ischemic and non-ischemic tissue. (A) Experimental design to analyze *in vivo* effects of TMyc and $TT1_{Ct}$. Permanent vessel occlusion and focal brain damage were induced in mice by cold-light irradiation after Rose Bengal i.v. injection. CPPs (3 nmol/g) were i.v. injected 1 h after damage initiation. Animals were sacrificed 5 or 24 h after injury onset as indicated. Representative 1 mm brain coronal slices stained with TTC after 24 h of insult are shown. (B) Immunohistochemistry of brain coronal sections prepared from TMyc-treated male animals 5 h after insult stained with isoform-specific TrkB antibodies (TrkB-FL and TrkB-T1), NeuN, GFAP and DAPI. Maximal projection of representative confocal microscopy images showing cortical areas of the infarct border are presented. Scale bar, 50 μm. (C) Analysis of $TT1_{Ct}$ delivery to male and female mice cortex after 5 h of ischemia. Bio-$TT1_{Ct}$ and Bio-TMyc were injected as before and detected in the contralateral region of coronal sections by Fluorescein Avidin D (green). Neuronal marker NeuN (magenta) is also shown. Peptide delivery was observed in neuronal (asterisks) and non-neuronal cells (arrowheads). Representative confocal microscopy images of cortical areas correspond to single sections. Scale bar, 20 μm.

Figure 6. Treatment with $TT1_{Ct}$ prevents reactive gliosis at early and late times of ischemic damage. (A) Coronal sections of male and female mice injected with TMyc or $TT1_{Ct}$ (3 nmol/g) after 5 h of insult were stained with antibodies for C3 (red), GFAP (magenta) and DAPI to

detect reactive astrocytes. Representative maximum intensity projection confocal images from the infarct border are shown. Scale bar, 20 μm. (B) Coronal sections of male mice treated with TMyc or $TT1_{Ct}$ (3 nmol/g) after 24 h of insult were stained as above. Representative maximum intensity projection of confocal images from the infarct border are shown. Scale bar, 20 μm. (C) Coronal sections of male mice injected with TMyc or $TT1_{Ct}$ (3 nmol/g) after 24 h of insult were stained with an antibody for CD68 (magenta) and DAPI to detect microglia and macrophage inflammatory state. Representative maximum intensity projection of confocal images from the contralateral cortex, infarct core and infarct border are shown. Scale bar, 20 μm. (D) Detail of cell morphology in selected areas indicated in panel C, corresponding to animals injected with TMyc as above indicated. Scale bar, 20 μm. (E) Coronal sections of male mice injected with TMyc or $TT1_{Ct}$ (3 nmol/g) after 24 h of insult were stained with antibody for Iba1 (red) and DAPI to detect microglia and macrophage inflammatory state. Representative maximum intensity projection of confocal images of the contralateral cortex, infarct core and infarct border are shown. Reactive microglia (asterisks) and resting microglia (arrows) were detected. Scale bar, 20 μm. (F) Detail of cell morphology in selected areas indicated in panel E, corresponding to animals injected with TMyc as above indicated. Scale bar, 20 μm. (G) Double immunohistochemistry with CD68 (green) and Iba1 (red) antibodies of the infarct core of male mice injected with TMyc or $TT1_{Ct}$ as above to analyze possible signal overlapping. Representative maximum intensity projection of confocal images are shown. Scale bar, 20 μm.

Figure 7. Treatment with $TT1_{Ct}$ reduces infarct volume and motor coordination deficits in animals exposed to permanent ischemia. (A and C) Infarct volume of animals injected with TMyc or $TT1_{Ct}$ (3 nmol/g) and sacrificed 24 h after damage induction, expressed as a percentage of the hemisphere volume. Individual data and box and whisker plots show interquartile range, median, minimum and maximum values. The mean value for each experimental group is also provided as a number on top of the corresponding plot. Results are given for the whole population (A) or disaggregated according to gender (C). Differences were analyzed by Student's *t*-test (n = 20 for A, n = 9-10 for C). (B and D) Evaluation of balance and motor coordination. Number of contralateral hind paw slips were measured in male and female animals. As above, results are presented for the whole population (B) or disaggregated according to gender (D). Differences were analyzed by Student's *t*-test (n = 21-22 for B, n = 10-12 for D). (E) Model proposed for $TT1_{Ct}$ action. In the presence of the control peptide TMyc, ischemic damage induces TrkB-T1 RIP and binding of particular proteins to the isoform-specific C-ter sequence, present in TrkB-T1-ICD or unprocessed full-length protein. This

excitotoxicity-induced binding results, by still undefined mechanisms, in shut-off of CREB and MEF2 promoter activities and transcriptional changes, affecting neurons and glial cells. Among other transcripts, the increase in TrkB-T1 and GFAP mRNA levels could contribute to decreased neuronal survival concurrent with increased microglia and astrocyte reactivity, resulting in bigger infarcts and a worse neurological outcome. In contrast, by interfering TrkB-T1 protein interactions, $TT1_{Ct}$ would help to maintain CREB and MEF2 activities and prevent the transcriptional changes induced by excitotoxicity, contributing to neuronal survival and reduced reactive gliosis. Consequently, the infarct size and the neurological damage would be strongly diminished.

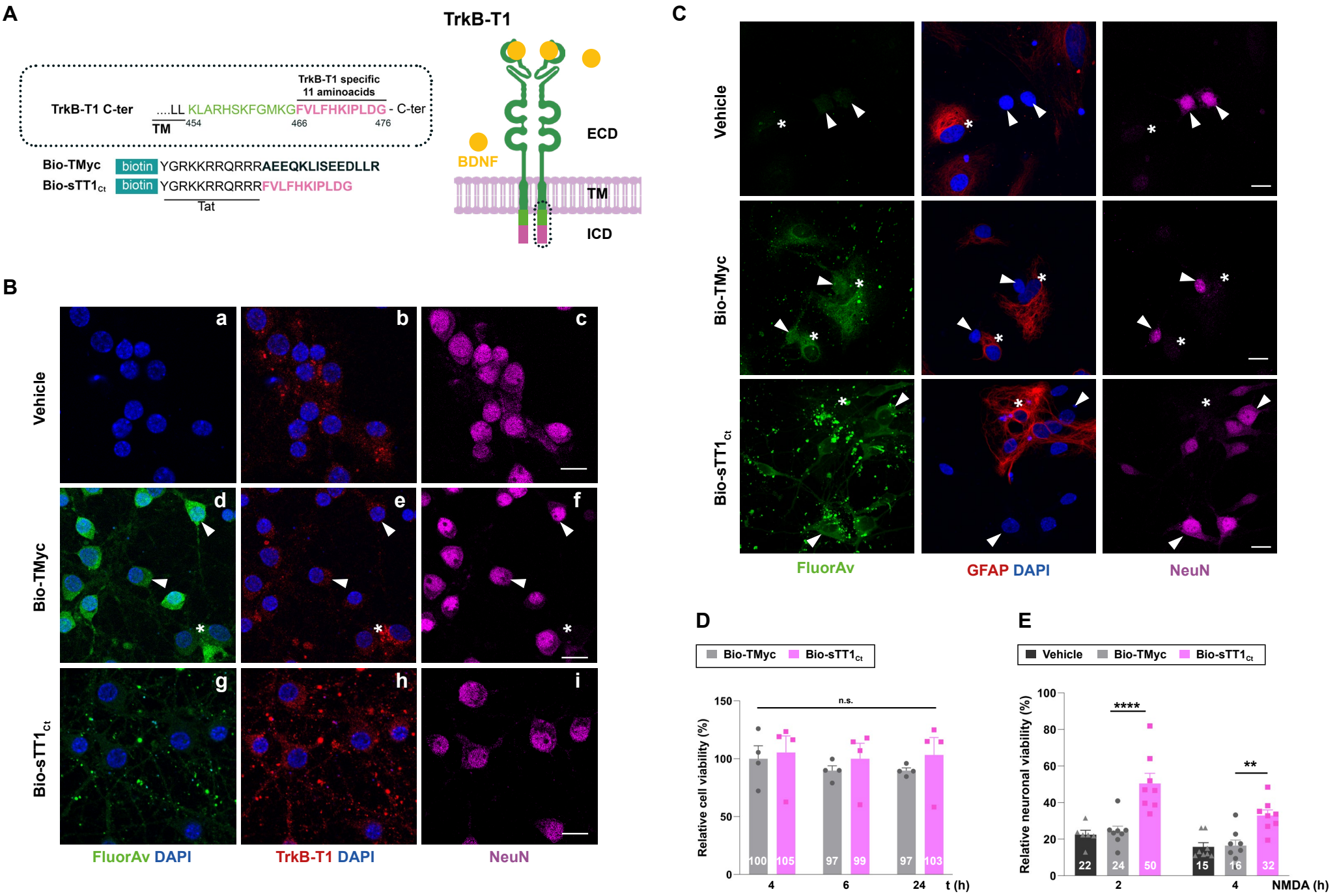

Figure 1. Validation of isoform-specific CPPs as tools for identification of TrkB-T1 interactome and prevention of neuronal death by excitotoxicity. (A) Structure of TrkB-T1 receptor, indicating the extracellular domain (ECD), responsible of brain derived neurotrophic factor (BDNF)-binding, the transmembrane segment (TM) and the short intracellular domain (ICD). The precise sequence corresponding to the TrkB-T1 C-ter (dotted oval) is indicated. It contains a region shared with TrkB-FL (black and green) followed by the TrkB-T1-specific sequence (pink). Biotin (Bio)-labelled Tat-derived CPPs, containing this isoform-specific sequence (Bio-sTT1$_{Ct}$) or unrelated sequences for the control peptide (Bio-TMyc), are also indicated. (B) Immunocytochemistry assays of primary cortical cultures treated with Bio-sTT1$_{Ct}$, Bio-TMyc (25 µM) or vehicle for 30 min. TrkB-T1 and Bio-sTT1$_{Ct}$ distribution were analyzed with an isoform specific antibody (red). Peptide visualization with Fluorescein Avidin D (green) shows that Bio-sTT1$_{Ct}$ presents a pattern similar to that observed for endogenous TrkB-T1. Bio-TMyc distribution was visualized in Neu+ (arrowheads) and Neu- (asterisk), corresponding respectively to neurons and presumably astrocytes (d-f). Scale bar, 10 µm. (C) Analysis of cultures treated as before with specific antibodies for astrocytes (GFAP, red) or neurons (NeuN, magenta). Peptide visualization with Fluorescein Avidin D (green) shows distribution in both Neu+ neurons (arrowheads) and GFAP+ astrocytes (asterisk). Scale bar, 10 µm. (D) Cell viability of cortical cultures treated with Bio-sTT1$_{Ct}$ and Bio-TMyc (25 µM) for 4, 6 or 24 h. Means ± SEM and individual points are presented relative to values obtained for 4 h of Bio-TMyc treatment (100%). Data were analyzed using two-way ANOVA test followed by *post hoc* Bonferroni test, $n = 4$. (E) Neuronal viability in cultures incubated with Bio-TMyc or Bio-sTT1$_{Ct}$ (25 µM) for 30 min and treated with NMDA for 2 or 4 h. Means ± SEM and individual points are presented relative to the values obtained for untreated cells (100%). Data were analyzed using two-way ANOVA test followed by *post hoc* Bonferroni test, $n = 8$.

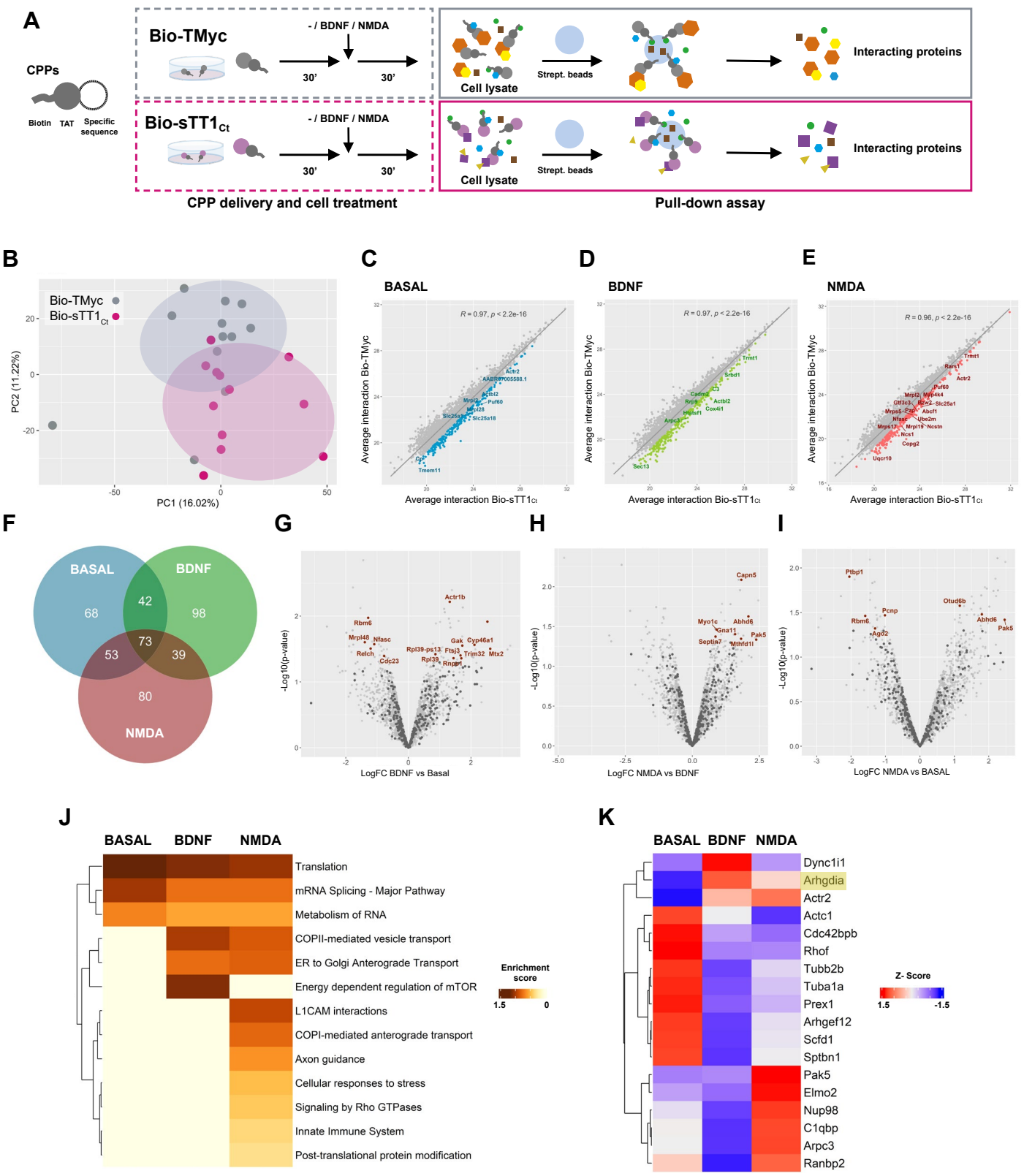

Figure 2. Bio-sTT1$_{Ct}$ as a tool to approach TrkB-T1 specific interactome in different biological conditions. (A) Experimental design of pull-down assays to isolate Bio-TMyc and Bio-sTT1$_{Ct}$ interacting proteins. Cultures were incubated with Bio-sTT1$_{Ct}$ or Bio-TMyc (25 µM) for 30 min before treatment with BDNF (100 ng/ml) or NMDA for 30 min. After that, cell lysates were combined with streptavidin agarose beads to isolate the CPP-interacting proteins. (B) Principal Component Analysis of Bio-TMyc and Bio-sTT1$_{Ct}$ pull-down isolates. Samples are represented using the first (PC1) and second (PC2) components of the analysis. (C-E) Pearson's correlation of the average protein interactions established by Bio-TMyc and Bio-sTT1$_{Ct}$ in basal conditions (C), or after BDNF (D) or NMDA treatment (E). Colored points represent the top 20% proteins whose residuals are furthest from the correlation line and have higher levels of binding to Bio-sTT1$_{Ct}$. (F) Venn diagram representing the number of proteins selected for each condition following the criteria described above. (G-H) Volcano plot presenting the results of the differential analysis of interacting proteins comparing BDNF vs basal conditions (G), NMDA vs BDNF (H) and NMDA vs basal conditions (I). Log_2FC and $-Log_{10}$(p-value) are shown. Proteins selected with the criteria explained above are represented as dark grey points while proteins showing statistically significant differences are labelled and presented as brown dots (p-value < 0.05). FDR = 9.52% (G), 4.15% (H) or 9.55% (I). FC, fold change. (I) Pathway enrichment analysis of selected proteins for basal, BDNF and NMDA conditions. A heatmap showing the enrichment score for each pathway (Reactome.db) at the different conditions is presented. (J) Comparison of RhoGDI (*Arhgdia*) (highlighted) and our selected proteins annotated in "Signaling by Rho GTPases" Reactome pathway in basal, BDNF and NMDA conditions. A heatmap showing the z-score indicating levels for each protein at the different conditions is presented.

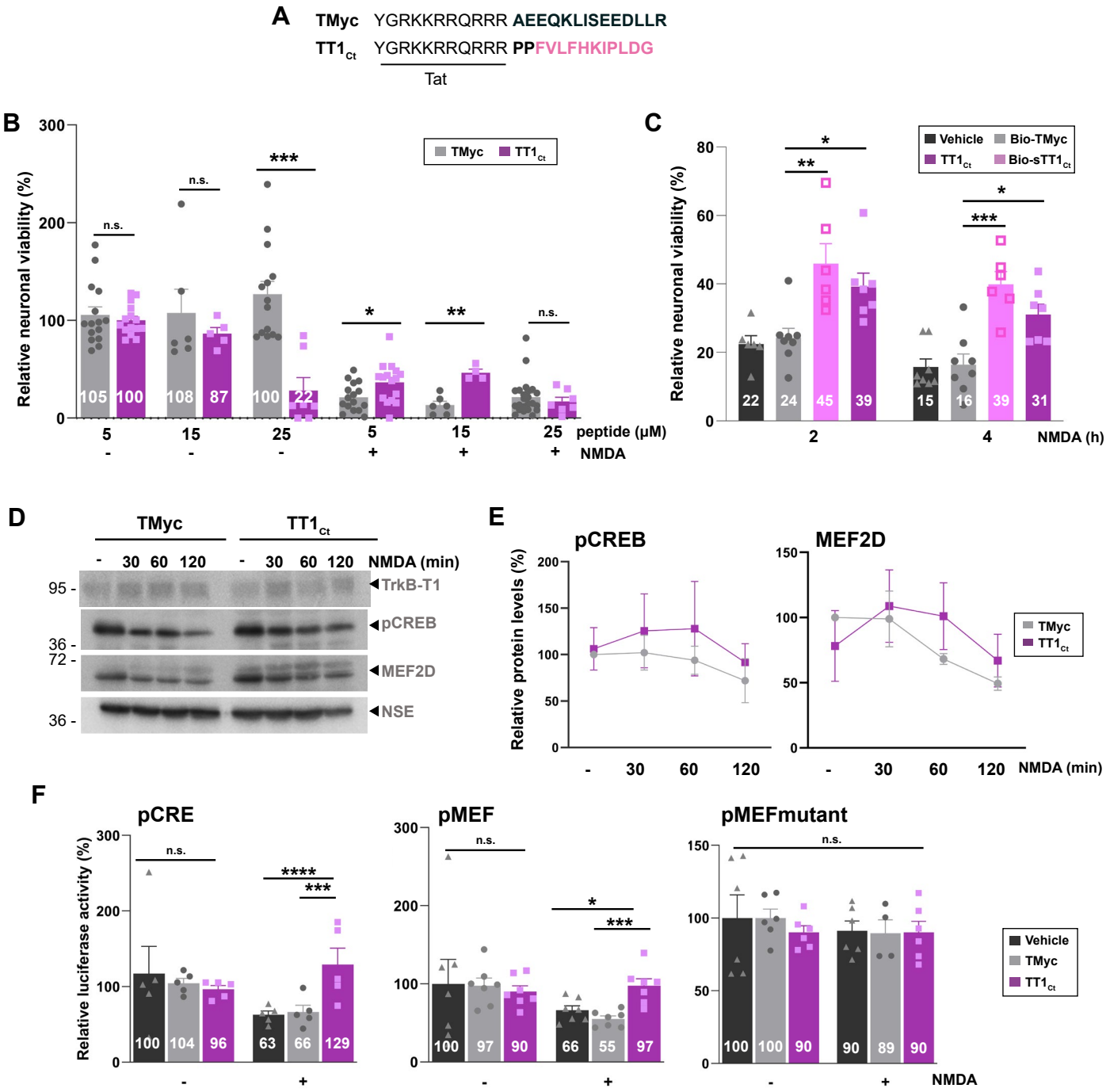

Figure 3. TrkB-T1-derived peptide $TT1_{Ct}$ is neuroprotective against *in vitro* excitotoxicity and prevents a decrease in CRE and MEF promoter activities induced by the excitotoxic injury. (A) Sequence of control peptide (TMyc) and TrkB-T1-derived CPP ($TT1_{Ct}$). (B) Neuronal viability in cultures incubated with TMyc or $TT1_{Ct}$ (5, 15 or 25 μM) for 30 min and then treated with NMDA (100 μM) for 2 h or left untreated. Individual data and means ± SEM are presented relative to values obtained in the untreated cells (100%). Data were analyzed using Kruskal-Wallis test followed by Mann-Whitney U-test, n = 6-16. (C) Neuronal viability in cultures incubated with Bio-TMyc, Bio-s$TT1_{Ct}$ or $TT1_{Ct}$ (15 μM) for 30 min and then treated with NMDA (100 μM) for 2 or 4 h. Individual data and means ± SEM are presented relative to values obtained for untreated cells (100%). Data were analyzed using two-way ANOVA test followed by *post hoc* Bonferroni test, n = 6-8. (D) Western Blot analysis of TrkB-T1, pCREB and MEF2D levels in cultures incubated with TMyc or $TT1_{Ct}$ (15 μM) for 30 min followed by treatment for 30, 60 or 120 min with NMDA. A representative experiment is shown. (E) Quantitation by densitometric analysis of pCREB and MEF2D levels. Means ± SEM are presented relative to basal conditions in the presence of TMyc (100%), n = 5. (F) Effect of excitotoxicity and $TT1_{Ct}$ treatment on CRE and MEF2 promoter activity. Cultures transfected with plasmids containing minimal CREB or MEF2 response elements (respectively, pCRE and pMEF) or pMEFmut were preincubated with peptides as above and treated with NMDA for 2 h or left untreated. Individual results and means ± SEM are presented relative to luciferase expression in untreated cultures. Data was analyzed by two-way ANOVA test followed by *post hoc* Bonferroni test, n = 5-7. For cultures transfected with pCRE and pMEF, treated with vehicle or TMyc, differences between -/+ NMDA are statistically significant although not shown for simplicity.

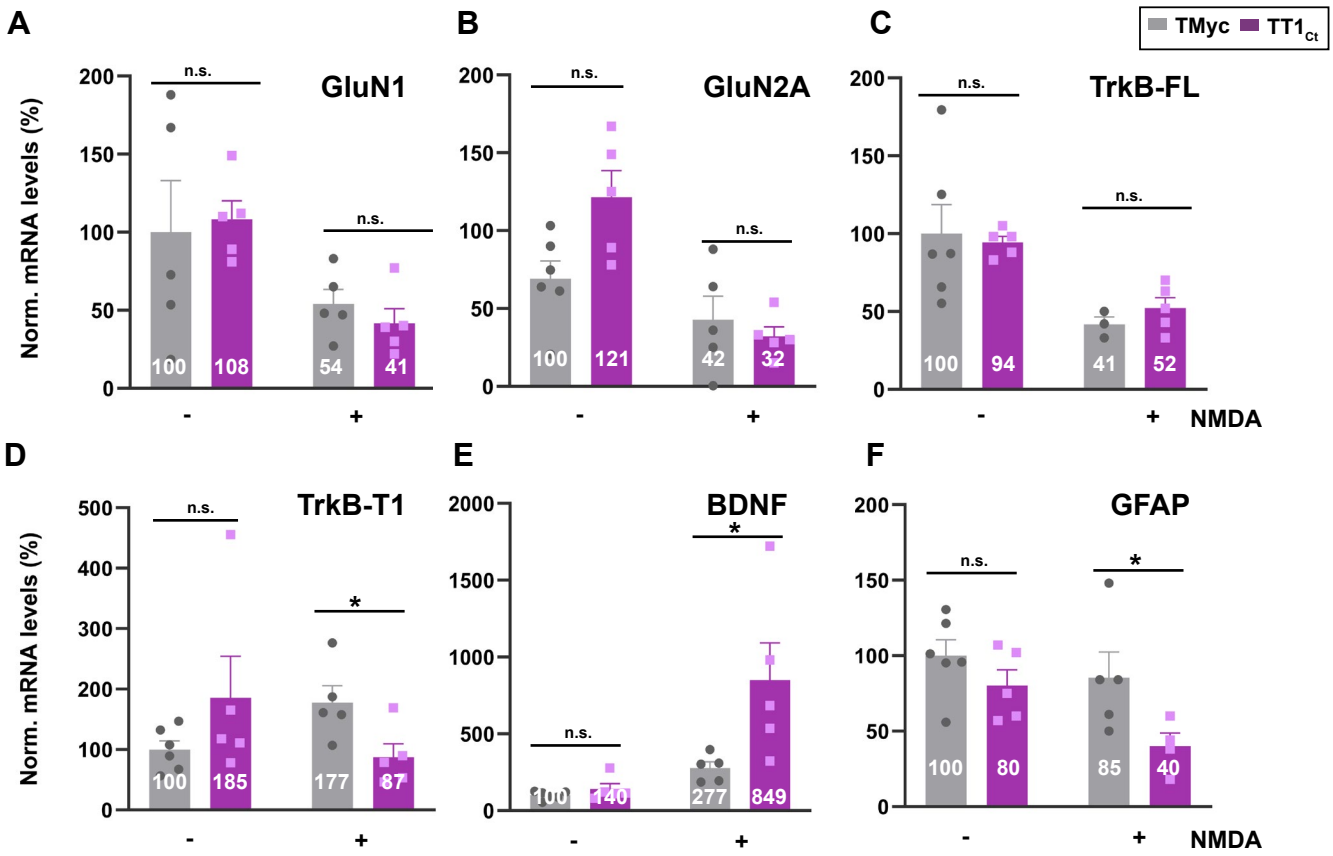

Figure 4. $TT1_{Ct}$ interferes transcriptional changes induced by excitotoxicity affecting expression of genes involved in survival/death choices. Cultures preincubated with $TT1_{Ct}$ or TMyc (15 µM) for 30 min were treated with NMDA for 4 h or left untreated. Levels of mRNAs encoding for NMDAR-subunits GluN1 (A) and GluN2A (B) or TrkB-FL (C) and TrkB-T1 isoforms (D) were normalized to those of NSE. Levels of BDNF (E) and GFAP mRNA (F) were normalized relative to GAPDH. Individual values and means ± SEM are presented relative to gene expression in cultures treated with TMyc (100%). Data were analyzed by two-way ANOVA test followed by *post hoc* Tukey's or Kruskal Wallis test followed by *post hoc* Dunn's test, $n = 5$.

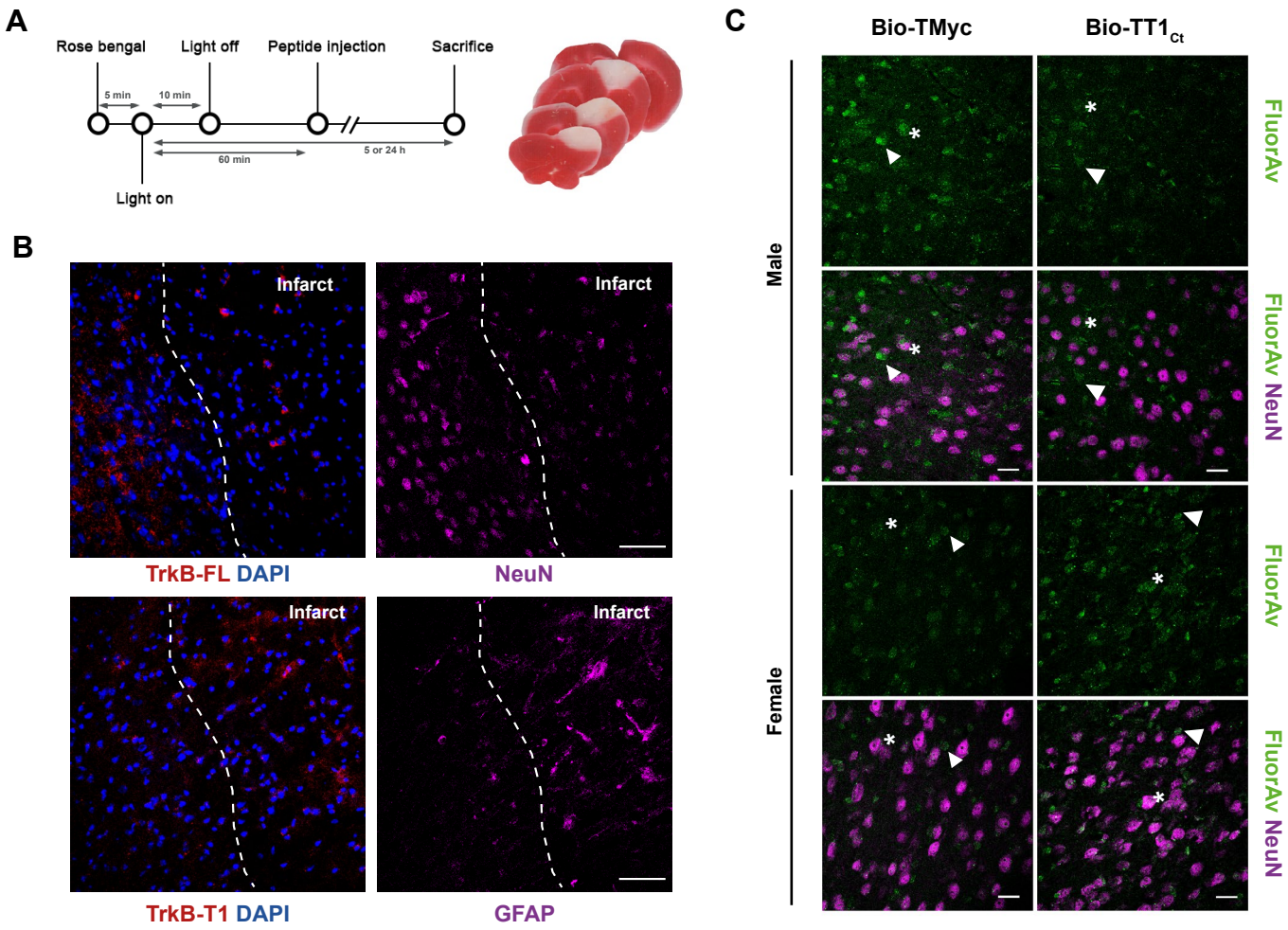

Figure 5. $TT1_{Ct}$ brain distribution in a mouse model of permanent ischemia showing upregulation of TrkB-T1+/GFAP+ cells in the interface between ischemic and non-ischemic tissue. (A) Experimental design to analyze *in vivo* effects of TMyc and $TT1_{Ct}$. Permanent vessel occlusion and focal brain damage were induced in mice by cold-light irradiation after Rose Bengal i.v. injection. CPPs (3 nmol/g) were i.v. injected 1 h after damage initiation. Animals were sacrificed 5 or 24 h after injury onset as indicated. Representative 1 mm brain coronal slices stained with TTC after 24 h of insult are shown. (B) Immunohistochemistry of brain coronal sections prepared from TMyc-treated male animals 5 h after insult stained with isoform-specific TrkB antibodies (TrkB-FL and TrkB-T1), NeuN, GFAP and DAPI. Maximal projection of representative confocal microscopy images showing cortical areas of the infarct border are presented. Scale bar, 50 μm. (C) Analysis of $TT1_{Ct}$ delivery to male and female mice cortex after 5 h of ischemia. Bio-$TT1_{Ct}$ and Bio-TMyc were injected as before and detected in the contralateral region of coronal sections by Fluorescein Avidin D (green). Neuronal marker NeuN (magenta) is also shown. Peptide delivery was observed in neuronal (asterisks) and non-neuronal cells (arrowheads). Representative confocal microscopy images of cortical areas correspond to single sections. Scale bar, 20 μm.

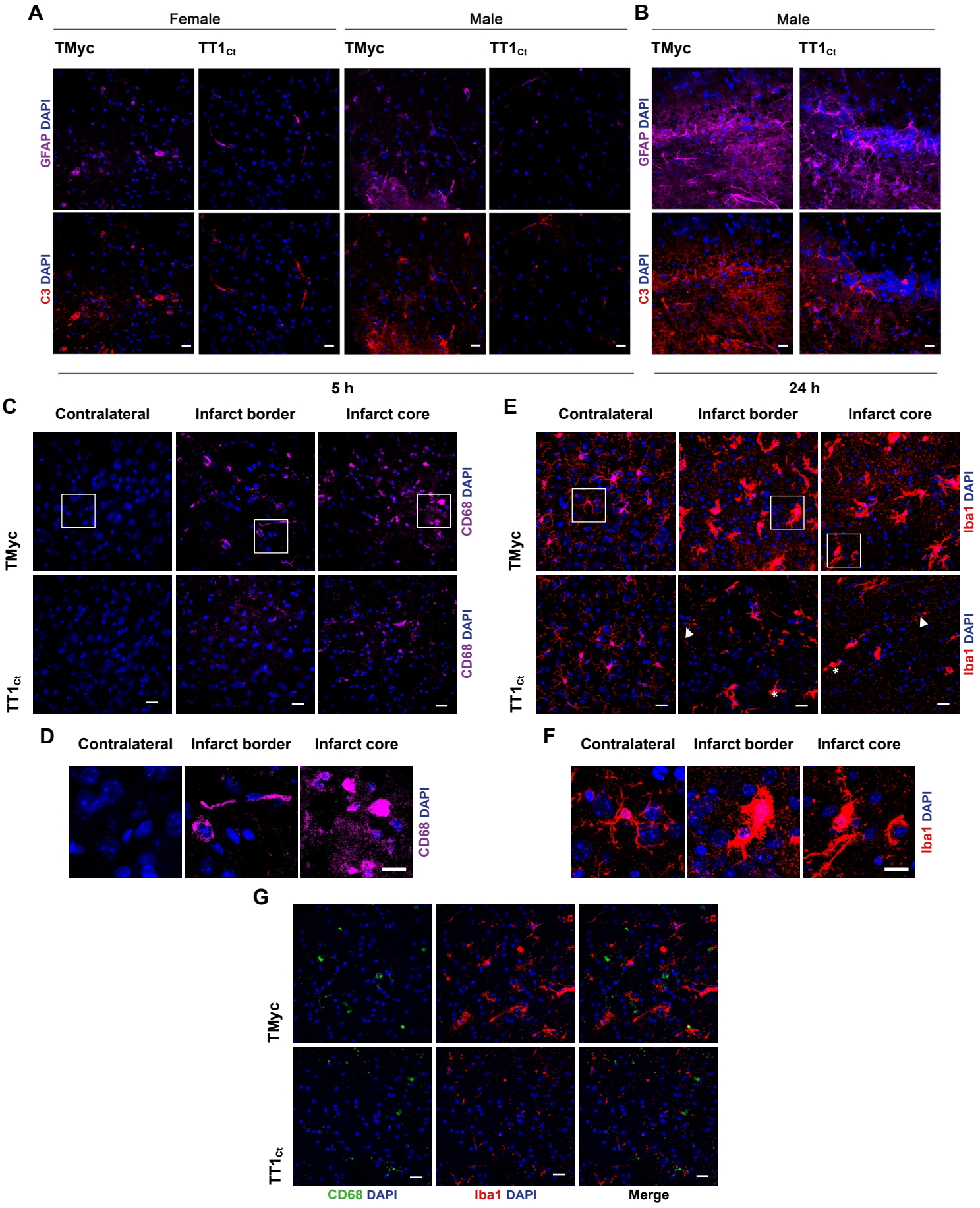
A
Female
Male
TMyc
TT1Ct
TMyc
TT1Ct
GFAP DAPI
C3 DAPI
B
Male
TMyc
TT1Ct
GFAP DAPI
C3 DAPI
5 h
24 h
C
Contralateral
Infarct border
Infarct core
TMyc
TT1Ct
CD68 DAPI
CD68 DAPI
E
Contralateral
Infarct border
Infarct core
TMyc
TT1Ct
Iba1 DAPI
Iba1 DAPI
D
Contralateral
Infarct border
Infarct core
CD68 DAPI
F
Contralateral
Infarct border
Infarct core
Iba1 DAPI
G
TMyc
TT1Ct
CD68 DAPI
Iba1 DAPI
Merge

Figure 6. Treatment with $TT1_{Ct}$ prevents reactive gliosis at early and late times of ischemic damage. (A) Coronal sections of male and female mice injected with TMyc or $TT1_{Ct}$ (3 nmol/g) after 5 h of insult were stained with antibodies for C3 (red), GFAP (magenta) and DAPI to detect reactive astrocytes. Representative maximum intensity projection confocal images from the infarct border are shown. Scale bar, 20 μm. (B) Coronal sections of male mice treated with TMyc or $TT1_{Ct}$ (3 nmol/g) after 24 h of insult were stained as above. Representative maximum intensity projection of confocal images from the infarct border are shown. Scale bar, 20 μm. (C) Coronal sections of male mice injected with TMyc or $TT1_{Ct}$ (3 nmol/g) after 24 h of insult were stained with an antibody for CD68 (magenta) and DAPI to detect microglia and macrophage inflammatory state. Representative maximum intensity projection of confocal images from the contralateral cortex, infarct core and infarct border are shown. Scale bar, 20 μm. (D) Detail of cell morphology in selected areas indicated in panel C, corresponding to animals injected with TMyc as above indicated. Scale bar, 20 μm. (E) Coronal sections of male mice injected with TMyc or $TT1_{Ct}$ (3 nmol/g) after 24 h of insult were stained with antibody for Iba1 (red) and DAPI to detect microglia and macrophage inflammatory state. Representative maximum intensity projection of confocal images of the contralateral cortex, infarct core and infarct border are shown. Reactive microglia (asterisks) and resting microglia (arrows) were detected. Scale bar, 20 μm. (F) Detail of cell morphology in selected areas indicated in panel E, corresponding to animals injected with TMyc as above indicated. Scale bar, 20 μm. (G) Double immunohistochemistry with CD68 (green) and Iba1 (red) antibodies of the infarct core of male mice injected with TMyc or $TT1_{Ct}$ as above to analyze possible signal overlapping. Representative maximum intensity projection of confocal images are shown. Scale bar, 20 μm.

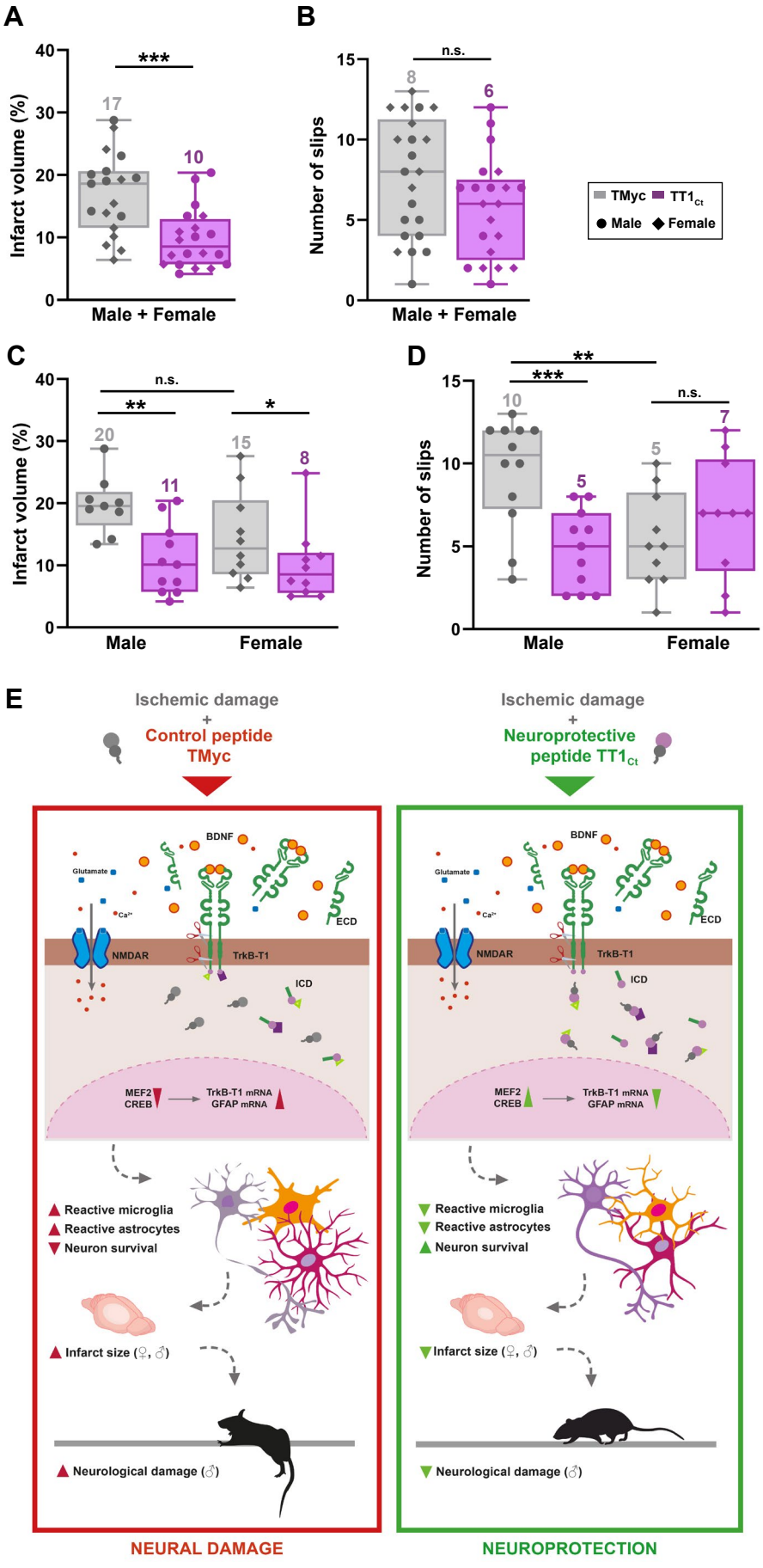

Figure 7. Treatment with $TT1_{Ct}$ reduces infarct volume and motor coordination deficits in animals exposed to permanent ischemia. (A and C) Infarct volume of animals injected with TMyc or $TT1_{Ct}$ (3 nmol/g) and sacrificed 24 h after damage induction, expressed as a percentage of the hemisphere volume. Individual data and box and whisker plots show interquartile range, median, minimum and maximum values. The mean value for each experimental group is also provided as a number on top of the corresponding plot. Results are given for the whole population (A) or disaggregated according to gender (C). Differences were analyzed by Student's *t*-test (n = 20 for A, n = 9-10 for C). (B and D) Evaluation of balance and motor coordination. Number of contralateral hind paw slips were measured in male and female animals. As above, results are presented for the whole population (B) or disaggregated according to gender (D). Differences were analyzed by Student's *t*-test (n = 21-22 for B, n = 10-12 for D). (E) Model proposed for $TT1_{Ct}$ action. In the presence of the control peptide TMyc, ischemic damage induces TrkB-T1 RIP and binding of particular proteins to the isoform-specific C-ter sequence, present in TrkB-T1-ICD or unprocessed full-length protein. This excitotoxicity-induced binding results, by still undefined mechanisms, in shut-off of CREB and MEF2 promoter activities and transcriptional changes, affecting neurons and glial cells. Among other transcripts, the increase in TrkB-T1 and GFAP mRNA levels could contribute to decreased neuronal survival concurrent with increased microglia and astrocyte reactivity, resulting in bigger infarcts and a worse neurological outcome. In contrast, by interfering TrkB-T1 protein interactions, $TT1_{Ct}$ would help to maintain CREB and MEF2 activities and prevent the transcriptional changes induced by excitotoxicity, contributing to neuronal survival and reduced reactive gliosis. Consequently, the infarct size and the neurological damage would be strongly diminished.